This is to certify that the
thesis entitled

THREE DIMENSIONAL FINITE ELEMENT ANALYSIS OF A SINGLE LAP BOLTED JOINT OF THICK ISOTROPIC MATERIALS

presented by

FLORIN IANCU

has been accepted towards fulfillment
of the requirements for the

MS degree in MECHANICAL ENGINEERING

Mary Lee Clouse P.E.
Major Professor's Signature

2 May 2003
Date

THREE DIMENSIONAL FINITE ELEMENT ANALYSIS OF A SINGLE LAP BOLTED JOINT OF THICK ISOTROPIC MATERIALS

By

Florin Iancu

A THESIS

Submitted to
Michigan State University
in partial fulfillment of the requirements
for the degree of

MASTER OF SCIENCE

Department of Mechanical Engineering

2003

ABSTRACT

THREE DIMENSIONAL FINITE ELEMENT ANALYSIS OF A SINGLE LAP BOLTED JOINT OF THICK ISOTROPIC MATERIALS

By

Florin Iancu

In addition to the development of new composite materials, there is a need for improving methods of joining these materials to other materials. Bolt-joining is often the most cost-effective. Mechanical joining of composite materials is not a very well understood domain and deeper investigation is required. This study concerns three dimensional investigations of the stresses along the bearing plane of an epoxy resin plate bolt-joined to a metallic one in a single lap. A finite element model was created and the results provided by it were verified experimentally. The experimental method used was embedded polariscope photoelasticity. Strain gages were also used to measure the strain at 3 points in the bearing plane. Comparison of the two sets of results showed that the FEA model is able to simulate with reasonable accuracy the behavior of the joint. The model was further used to investigate two simple methods of decreasing the highest stress in the composite plate.

to my sister, Mirela

ACKNOWLEDGEMENTS

I offer my sincerest appreciation to Dr. Gary L. Cloud for giving me the opportunity to work on this project and for his continuous advice and support. I also thank Dr. Andre Benard and Dr. Dahsin Liu for their interest in the research, and my colleague, Xu Ding for the help with all the experiments performed during the work on this project. Last, but not least, I thank Dr. Brian S. Thompson for the life advice that he offered me during my study as a master student at Michigan State University. To all of the above, THANK YOU.

TABLE OF CONTENTS

LIST OF TABLES

LIST OF FIGURES

KEY TO SYMBOLS

σ_1, σ_2 – principal stresses

τ_{12} – shear stress

τ_{FEM} – shear stress obtained numerically

τ_{exp} – shear stress obtained experimentally

ε – error

n_1, n_2 – refractive indices of materials

n_0 – refractive index of the medium

C_1, C_2 – absolute photoelastic coefficients

C_σ – photoelastic coefficient

d, δ – thickness

λ – wavelength

N – fringe order

A – cross-sectional area

F, L – applied load

T – installation torque

K – torque coefficient

D – nominal bolt diameter

P – clamp load objective

E – Young's elasticity modulus

ν – Poisson ratio

Chapter 1

INTRODUCTION

Fastening and joining are acts of bringing together, connecting or becoming a unit. From almost the dawn of time, man has used his ingenuity to connect and fasten different materials. (Parmley 1977)

Nowadays, there is a wide range of processes covering mechanical fastening. Yet, in spite of the research that has been done in the past 100 years, not everything about fastening materials has been researched or covered. In the field of composites, because of the tremendous surge in material development, the research surface has been barely scratched (Lincoln, Gomes et al. 1984).

Fastening by bolts is, perhaps, the most widely spread method of fastening. That is because it is a non-permanent joint, is easy to set up in most conditions and, most of the time, does not require manufacturing of special parts, which makes it less expensive.

As technology develops rapidly, new and better materials need to be incorporated into old and new structures. Such cases are in aerospace,

automotive, defense and sporting goods industries and, even construction. The problem of fastening composite materials using bolted joints is a very delicate one. Often the composite materials are glued in place; but in aerospace and automotive industries, non-permanent joints are needed, so parts can be inspected and/or replaced. An example of fastening a composite panel to a metallic frame using a bolt can be seen in Figure 1.1.

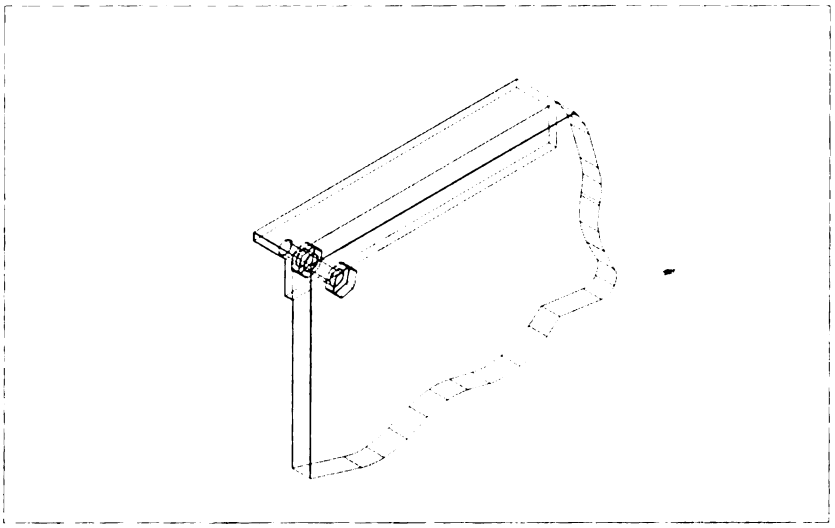

Figure 1.1. Fastening a composite panel to a metallic frame.

In bolted composite structures, stress concentrations develop around the holes, severely reducing the strength and fatigue life of the structure. To utilize the full potential of fiber reinforced polymers (FRP) in structural elements, appropriate methods for stress and failure analysis must be developed. The strength of a bolted joint depends on many factors, including joint type and

geometry, bolt size, bolt tension, hole tolerance, washer size, roughness of the surfaces, fiber type and form, resin type, and fiber/resin volume ratio.

The trends and results of the current research in this domain are presented briefly in the following literature review.

1.1. LITERATURE REVIEW

The extant literature on joining composite materials has evolved under three main streams: one would be the experimental investigations of failure of the joint or comparison of different types of joints; the second one is investigations of stresses and strains near the joint, and the third one, which has been facilitated by the developments in computer science, consists of creating numerical models for easier study of the joint. The most recent technique in the numerical modeling stream is finite element analysis.

Most of the techniques used to analyze the stresses and strains of the specimens joined together are surface techniques, they can not predict what is happening inside the specimen. So in order to be able to predict more

accurately, thin specimens were used, such that the variation of the stresses and strains from the surface to the middle would be small.

1.1.1. Experimental studies

Most of the experimental research done in the domain of bolted joints dealt with the failure of the joint. Several modes of failure were observed, studied, and classified as shown in Figure 1.2:

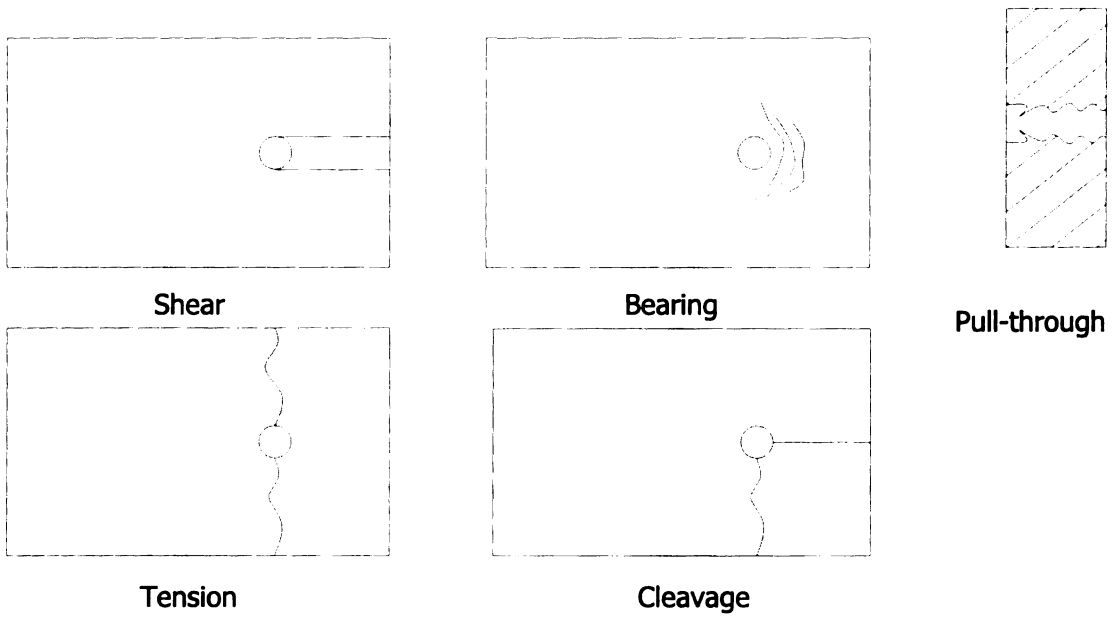

Figure 1.2. Failure modes of a bolted plate in tension.

These modes are characteristic to bolt joints in general. Several failure modes characteristic of laminated composite materials were analyzed, including:

- matrix cracking
- fiber fracture
- delamination
- kinking

Single-lap bolted joining of materials forms only a small fraction of the research done in the past on mechanical joining of materials. Mo st of the research deals with double-lap bolt joints. However single-lap bolt joint are the most commonly used for their low cost and simplicity. But the extant research has been done on a joint geometry that is little used (double-lap), and the reason for this is that single-lap joint is difficult to investigate either experimentally or numerically. Certainly, further investigation of single-lap joints is needed.

Camanho and Matthews (Camanho and Matthews 1996) summarized the previous work in predicting the failure of bolted joints in composites in their work on stress analysis and strength prediction of mechanically fastened joints in FRP. The conclusion was that by taking the composite to the ultimate load, very little information can be extracted. They suggested that a three dimensional model of the joint needs to be studied further. Also, the failure of the composite plate is

affected by the friction, clearance, and the contact area between the bolt and the interior surface of the hole.

Ireman, Ranvik and Ericksson adopted a different approach on the failure problem of a composite plate joined with a bolt (Ireman, Ranvik et al. 2000). Using loading in quasi-static cycles, damage development around the hole was detected using such methods as strain measurement, acoustic emission, X-ray, and microscopic examination.

The results showed that specimens with countersunk fasteners have lower strength than the corresponding specimens with protruding head fasteners. This effect is less pronounced for joints involving thicker laminates.

As expected, the specimens with torque-tightened bolts have significantly higher failure loads than corresponding specimens without bolt torque. The reason for this is that a considerable part of the load is transferred by friction in a joint with torque-tightened fasteners, and the clamping also introduces a lateral constraint in the washer area, which prevents delamination.

Dano, Gendron, and Picard (Dano, Gendron et al. 2000) developed a finite element model to predict the response of pin–loaded composite plates. Their model took into account contact at the pin-hole interface, progressive damage, large deformation theory, and a non-linear shear stress-strain relationship. They concluded that when the shear stress-strain relationship is linear, the use of the

maximum stress criterion for fiber failure leads to a higher and more realistic strength than Hashin's criterion. When a non-linear relationship is considered, the predictions from the different failure analyses converged toward the same result.

In their paper, "On design of joints between composite profiles for bridge deck applications" Zetterberg, Astrom, Backlund and Burman (Zetterberg, Astrom et al. 2001) make a comparison between adhesively bonded and bolted joints of pultruded composite profiles for a bridge-deck. The design consists of a row of bolts for the upper joint and two rows for the lower one. The upper joint is a single-lap joint, while the lower one is double-lap joint. Regarding the bolted joints, the results showed that an extra row of bolts would not increase the joint load capacity, but the upper joint could have a smaller number of bolts than the lower one. Washers as large as possible in diameter (no less than 20mm) should be used. Bolts should be tightened with a controlled torque, which should be as large as possible without damaging the laminate.

Matthews (Matthews 1983) experimented with double-lap bolted joints of composite plates. He studied different types of materials and the influence of the joint parameters on the bearing stress and the specific strength. The parameters that he took into account included bolt diameter, end distance, bolt hole clearance, and bolt tension.

Also, he ran experiments with single bolt joints and multi-bolt joints. From his conclusions, the following are most motivating. The strength rises as e/d increases (where e is the end distance and d is the hole diameter). Bearing stress is reduced up to 40% if the bolt is only finger tightened. Bearing stress increases as d/t falls for finger tightened bolts, but the opposite effect is seen for fully tightened bolts (t is the thickness of the plate).

Another experimental study was done by Starikov and Schon (Starikov and Schon 2001) to differentiate the behavior of composite bolted joints in tension and in compression. The joint plates were made of quasi-isotropic and 0°-dominated lay-ups and fastened by two, four, and six titanium bolts. Two configurations were tested: single and double-lap joints. The obtained experimental results showed that bolted joints with four and six bolts had higher resistance to quasi-static loading than joints with two bolts. Generally, the compressive strength was higher than the tensile strength for the same specimen type. This was explained by load being transferred through the bolt, which reduces the stress concentration at the bolt hole. Bolt movement measurements under quasi-static loading showed that there were different stages of bolt movement due to the influence of friction between the composite plates, bolt tilting, sliding, and bolt bending. The strain evolution was affected by the bolt behavior. The load transfer measurements between different bolt rows

showed that, in most cases, the first row of bolts transfers the largest amount of the load.

Park (Park 2001) studied the effects of stacking sequence and clamping force on delamination bearing strength and ultimate bearing strength of mechanically fastened joints (pinned and bolted) in carbon/epoxy composite laminates using the acoustic emission (AE) technique. The AE technique was used to detect the onset of delamination failure of composite laminates. The most important conclusions of his study are the following. The stacking sequence of the lay-up $[0_6/90_6]_s$ with 90° layers on the surface is more advantageous than the lay-up $[0_6/90_6]_s$ with 0° layers on the surface, from the point of view of delamination in the bearing plane. The stacking sequence of $[90_3/0_3/\pm45_3]_s$ has the highest delamination bearing strength and the second highest ultimate bearing strength and should be preferred to the lay-ups $[90_3/\pm45_3/0_3]_s$ and $[0_3/\pm45_3/90_3]_s$, from the viewpoint of desirable fail-safe delamination failure. Thus, the 90° layers play an important role in the delamination bearing strength of composite laminates. The delamination bearing strength of the lay-up with 90° layers on the surface is stronger than the one with 90° layers in the middle of the laminate. The lateral clamping pressure suppresses the onset of delamination and continuously suppresses the propagation of interlaminar cracks.

Regarding the fatigue of composite joints, Starikov and Schon add their contribution with two experimental works (Starikov and Schon 2002; Starikov and Schon 2002). They performed fatigue tests on carbon/epoxy composite materials with quasi-isotropic and 0°-dominated lay-ups. The tests were carried out under cyclic loading with stress ratio R=-1. Strain gage measurements were done to analyze surface strain distribution and load transfer between bolt rows. Extensometers were used to measure relative displacement between the composite plates. Based on all their tests, some conclusions can be drawn. Single and double-lap joints with a quasi-isotropic lay-up and fastened by six bolts displayed the highest resistance to fatigue, whereas the shortest fatigue life was exhibited by single row joints. Bolt failure was the dominant mode for joint failure, however for high loads, the joints failed in two modes. The fatigue behavior of the composite joints depends linearly in the number of bolts. Extensometer measurements show that there is a subtle increase in relative displacement between the specimen plates due to fatigue damage in the joint system. Bolt movement was found to increase measurably during fatigue testing. Changes in the bolt behavior occur very early in the fatigue life of bolted joints and reflect rapid changes in the damage state of the fastener system and the adjacent composite. Optical fractography showed that bolted laminates subjected to high applied loads sustained severe damage around the bolt holes.

Bolt-hole clearance effects were investigated by McCarthy, Lawlor, Stanley, and McCarthy (McCarthy, Lawlor et al. 2002). For a single bolt, single-lap joint, four clearances were studied, ranging from zero tolerance to 240 μm. The specimens were manufactured from graphite/epoxy HTA/6376, with quasi-isotropic and 0° dominated lay-ups. Protruding head and countersunk bolts were used, with two different applied torque levels. Increasing clearance was found to result in reduced joint stiffness and increased ultimate strain in all configurations. Finger-tightened joints with protruding head bolts showed a link between clearance and strength, but countersunk and torque-tightened joints did not. A delay in load take-up also occurred with higher clearance joints, which has implications for load distributions in multi-bolt joints.

Wang and Sheu (Wang and Sheu 1996) in their experimental and numerical analysis in 1996 used a birefringent coating to perform reflective photoelasticity. The fringes obtained by capturing images with a CCD camera were further processed to divide each fringe in fractions, thus obtaining a more accurate stress value. The geometric effects (different edge distances and widths) on the surface stress distribution around the bolted joints were investigated. Experimental results showed that the assumption of cosine normal load distribution underestimated the radial stresses near the hole boundary. Maximum shear stresses, which caused most failures in unidirectional composites, were located between 30° and 50° measured from the bearing plane.

An extreme case of failure was studied by Tong (Tong 2000). He examined the impact of the position of the bolt, and the washer on bearing failure behavior of joints with lateral constraints. The specimen plate was placed between two steel plates, and the washers were placed on each side of the composite plate. Two extreme diametral fit positions, with a negative or positive bolt-hole-to-washer clearance, were considered. When the washers are placed to their extreme positions in the loading direction, there is an unconstrained gap between the bolt and the washers, which generates lower initial failure. But there is no difference in the ultimate failure loads between the bolted joints with washers located in the two extreme positions.

1.1.2. Numerical modeling

Although numerical models of mechanical joints have been created before, only a small part of them investigated three dimensional stress state. More common was the two dimensional analysis of a bolted joint.

Among the first finite element models created for studying contact stresses were the ones of Chen, Lee, and Yeh in 1995 (Chen, Lee et al. 1995). The analysis was based on an incremental variational principle and the

transformation matrix derived from three-dimensional contact kinematics conditions. The model took into account the effects of friction, clearance, bolt elasticity, stacking sequence, and contact tractions around the bolted joint.

Other finite element models for laminate composite joints were developed by Barbero, Luciano, and Sacco (Barbero, Luciano et al. 1995). In their paper a contact/friction, isoparametric, finite element for the analysis of connections between laminated composite plates is presented. The element is compatible with a three dimensional plate element based on layer-wise constant shear theory. The contact/friction element is based on regularization of the unilateral contact with an orthotropic Coulomb friction problem. Two different friction coefficients in orthogonal directions and a constitutive law to model slip in any direction are used to account for the orthotropic surface texture of fiber reinforced materials. The contact and friction constitutive law is distributed uniformly over the entire surface regardless of mesh refinement or element distortion. The simulated behavior of the joint is very close to the real behavior of a composite joint, including complete slip of a plate relative to the other.

For failure prediction using finite element analysis, Sawicki and Minguet created a model using a commercial finite element package (Savicki and Minguet 1997). Samtech's SAMCEF-BOLT finite element package was used to investigate failure mechanisms and to develop a strength prediction methodology. The 2-D

finite element model consisted of a symmetric laminated plate containing a hole, and a rigid, frictionless pin in the hole. The Tsai-Wu, ply-level, quadratic failure theory was utilized to predict element failure; transverse tension and compression failure modes were suppressed to provide more representative interaction envelopes in the compression regime. The model was calibrated semi-empirically using open hole compression data for one lay-up. Subsequently, open and filled hole compression strength predictions were generated for different lay-ups. SAMCEF-BOLT predictions were shown to be consistent with the experimental data. The observations and conclusions obtained were the following: compression performance of 0.250" and 0.251" diameter filled holes was very similar; but 0.253" diameter strengths were lower due to the lower percentage of load transferred through the fastener at failure. Fastener hole-filling and through-thickness stabilization (provided by the fastener head and collar) were the key factors governing filled hole compression strength. Clamp-up torque, apparently, had little effect. All filled-hole specimens exhibited development of a through-fastener load path and, subsequently, higher strengths than open-hole specimens.

The failure analysis of bolted connections of glass woven fabric composites was the topic of Lin and Tsai's research (Lin and Tsai 1995) which involved both experimental work and finite element analysis. Two types of specimens were investigated; some having drilled holes and the rest having molded-in holes. The

failure mode and failure strength of $[0/90]_s$ and $[\pm 45]_s$ laminates with various hole diameters and values of *e/d* were considered (where *e* is the distance from the center of the hole to the edge of the plate and *d* is the diameter of the hole). Experiments showed that specimens with molded-in holes are stronger when the edge distance is small (*e/d*=1), while for larger *e/d* ratio the two types of specimens have almost the same strength. In numerical failure analysis, the finite element method, combined with Hashin quadratic criterion provided results similar to the experimental ones, except for *e/d*=1.

Ramakrishna, Hamada, and Nishwaki investigated, experimentally and numerically, the tensile behavior of bolted joints of pultruded sandwich composite laminates (Ramakrishna, Hamada et al. 1995). In general both the failure mode and the joint strength of longitudinal specimens were independent of the joint geometry. These results were predicted with reasonable accuracy by the finite element analysis method. In the case of transverse specimens, the failure mode changed from net tension to bearing mode with increasing w/d ratio (w is the width of the plate and d is the diameter of the hole). The failure strength increased with w/d ratio from 2 to 7. So, the joint efficiency was higher in the pultrusion direction than in the transverse direction.

Optimum bolted joints for composite materials, glass/epoxy, and carbon/epoxy under tensile loading were investigated by Oh, Kim, and Lee (Oh,

Kim et al. 1997). The design parameters considered for the bolted joints were ply angle, stacking sequence, ratio of fiber/resin, the outer diameters of washers, and clamping pressure. The specimen was designed to undergo bearing failure only. To assess the delamination of the composite materials, a three-dimensional stress analysis of the bolted joint was performed using a commercial finite element package and compared with the experimental results. On the finite element model, a cosine load distribution was used for the contact force between the bolt and the composite. Only a quarter of the plate was modeled, due to symmetry, and solid elements from ANSYS library were used. Among the conclusions drawn by the authors, the comparison between experimental and numerical results is to be noted. The finite element analysis predicted the first peak load due to delamination on the y-direction but was not able to predict the maximum failure load. For a more accurate prediction of the joint strength, it might be necessary to include in the model the effects of the material non-linearity, friction between the washer and laminate, and stiffness reduction caused by failure of some layers.

A three-dimensional finite element model of bolted composite joints was developed by Ireman (Ireman 1998) to determine the non-uniform stress through the thickness of the composite laminates in the vicinity of a bolt hole. The numerical model results were compared with experimental results obtained by strain gage measurement. Some conclusions can be drawn from this study.

Torque tightening reduced the strain level compared with finger tightening. Higher strain levels were generally observed in the specimens with countersunk bolts compared with specimens with protruding head bolts. Although in the finite element model some assumptions were made, the results generally agreed with the experimental ones. Ireman considers that the discrepancies come from limitations in the friction coefficient used, which has to be assumed on the basis of friction coefficient measured at the fracture surface. Ireman believes that the friction coefficient for material combinations used in composite bolted joints are therefore an important subject in future research.

Chapter 2

RESEARCH OBJECTIVES

As described in section 1.1, the research done so far included mostly two dimensional FEA models that simulated the bolted joint. Only a small number of these models were of single-lap joints, most being of double-lap joints. Most of them modeled only the plates, the fastening being simulated as external loads applied directly to the plates. Some fastening forces were modeled as thermal loads applied to the fastener. All the FEA models were verified with strain gage measurements.

This research studies a single-lap joint of thick plates, by modeling it numerically with finite element analysis. The model includes the fastening system composed of the bolt-washer and nut-washer units. The numerical results are compared with the experimental data, which was obtained through two methods: photoelasticity and strain gage measurements. As can be seen in Figure 1.2, most of the failure cases involve the bearing plane; this is why the analysis is concentrated on that plane of the polymer plate. The position and magnitude of the maximum stress is identified inside the composite plate.

Several alternative designs of this plate were studied numerically to analyze the changes in its behavior.

The numerical model yields a three dimensional map of the stresses and strains inside the photoelastic plate. The experimental methods used are able to provide information from inside the plate. All the measurements are made on the bearing plane of the photoelastic plate. The specimen investigated is made out of isotropic material, and future research will be concentrated on repeating the analysis for laminated composite materials.

The three methods used in this study were chosen for a number of reasons. The finite element analysis provides results much cheaper and faster than experiments. For creating a reliable FEA model, first, a model that can be verified experimentally has to be created. Then, improvements of that model can be simulated, and qualitative as well as quantitative results can be obtained.

The photoelasticity method was used for having the advantage of being the only experimental method able to provide directly the values of stresses. The disadvantage of using an embedded polariscope is that the Tardy goniometric compensation method for fringe fraction measurements cannot be used. Because of this, the results obtained by experiment have a significant error margin.

Strain gages were chosen for their accurate response, relative ease of use and low cost. The relation between the strain measured by strain gages and the stress measured by photoelasticity can be easily verified.

The remainder of this thesis is organized as follows. The experimental methods used to obtain information about the shear stress and the strain on the bearing plane of the photoelastic plate are presented in chapter 3. This chapter also covers the calibration of the material that was performed and some other experiments necessary to obtain information for creating the FEA model. Chapter 4 describes in detail the FEA model of the single-lap bolted joint. Chapter 5 presents the numerical results and compares these results with the experimental ones. Several loading cases were compared: single-lap pin connected joint and bolt connected joint, with different fastening torques on the bolt. In chapter 6, some alternatives are proposed for the photoelastic plate and a discussion of how the changes proposed affect the results.

The most difficult problem when dealing with finite element modeling of a joint resides in the necessity of creating contact surfaces. The parameters of the contact surface will greatly affect the final result. The problem becomes even more complicated when we are dealing with non isotropic materials. The second problem when trying to create an FEA model of the single-lap joint is simulating

the fastening force (torque applied to the bolt and nut). A brief explanation of these two problems and the solutions generated are described in section 4.1.

The load cases studied are as follows: pin connected - the two plates are joined by a pin and an extension force is applied on the end of one plate, while the other plate is fixed on the direction of the extension; the pin was replaced by a bolt and the joint was studied for several magnitudes of torque applied to the bolt-nut pair: finger tightening (approx. 3 in-lbs of torque), 25 in-lbs torque and 40 in-lbs torque.

Chapter 3

EXPERIMENTAL METHODS

Since the topic of this research is numerical analysis, the experimental investigations will be described only briefly. Their description and the results obtained are needed to create the comparison between the numerical and experimental results. The experimental investigations were performed together with Xu Ding, as part of the comprehensive research program.

To perform the experimental investigations on the single-lap joint two methods were used: the photoelasticity method was used to find the shear stress distribution in the bearing plane, and resistance strain gages were employed for measuring strain in the same plane. For the photoelasticity method, the stress-optic coefficient of the epoxy resin needed to be determined first. Other experiments were performed to obtain data needed as input to the FEA model. Friction coefficients as well as fastening force were determined.

3.1. PHOTOELASTICITY

3.1.1. The concept of photoelasticity

In its essence, the photoelasticity technique is a classic interferometric technique. The surface of the specimen acts as a beam splitter because it divides the incident light into orthogonally polarized components (thus the need for a birefringent material). Birefringence is the variation of the refractive index with the direction of polarization and propagation axis, so light polarized in one plane travels with a different speed than light polarized in another plane. The two orthogonal components travel the same physical distance (the model thickness), but their path lengths differ because of the difference in refractive index. These variations are induced by stress. So, the polarized waves have a relative phase difference when they exit the specimen. The phase difference is converted into amplitude information through interference, as the two components are recombined at the analyzer. (Cloud 1995)

Photoelasticity theory involves the observation of fringe patterns for determination of the stress-induced birefringence. Let σ_1 and σ_2 be the principal stresses at a point. The principal axes of refraction correspond to the principal stress axes. Each principal index of refraction is a function of the two stresses (eq. 3.1).

$$\frac{n_1 - n_0}{n_0} = C_1\sigma_1 + C_2\sigma_2$$
$$\frac{n_2 - n_0}{n_0} = C_2\sigma_1 + C_1\sigma_2 \qquad (3.1)$$

where C_1 and C_2 are the absolute photoelastic coefficients

n_1 and n_2 are the indices of refraction of the plate on the two directions

n_0 is the index of refraction of the medium in which the plate is immersed

we let

$$C_\sigma = C_1 - C_2 \qquad (3.2)$$

to obtain:

$$\frac{n_1 - n_2}{n_0} = C_\sigma \cdot (\sigma_1 - \sigma_2) \qquad (3.3)$$

Along any isochromatic fringe (locus of points where the difference between relative refractive indices multiplied by the thickness is an integral multiple of the wavelength of the radiation).

$$\left(\frac{n_1 - n_2}{n_0}\right) \cdot d = N \cdot \lambda \tag{3.4}$$

where N is the fringe order

λ is the wavelength of the radiation

d is the thickness of the plate

The final result is

$$\sigma_1 - \sigma_2 = 2 \cdot \tau_{12} = \frac{N \cdot \lambda}{d \cdot C_\sigma} \tag{3.5}$$

As can be seen from the formula above, the experiment provides us with a map of twice the maximum shear stress averaged on the thickness of the specimen.

In order to perform a photoelastic investigation, the following items are needed: a collimated light field and two polarizers. One polarizer is placed in front of the specimen and the other behind it. Light polarized in the first polarizer's plane enters the specimen. The light wave is split into two components that propagate through the specimen at different velocities. The two waves are recombined in the second polarizer where they are able to interfere with each other. These are the basic components of a polariscope.

A schematic of a whole field photoelastic polariscope is presented in the Figure 3.1, together with the details of it, along with the exact components used for the experimental measurements.

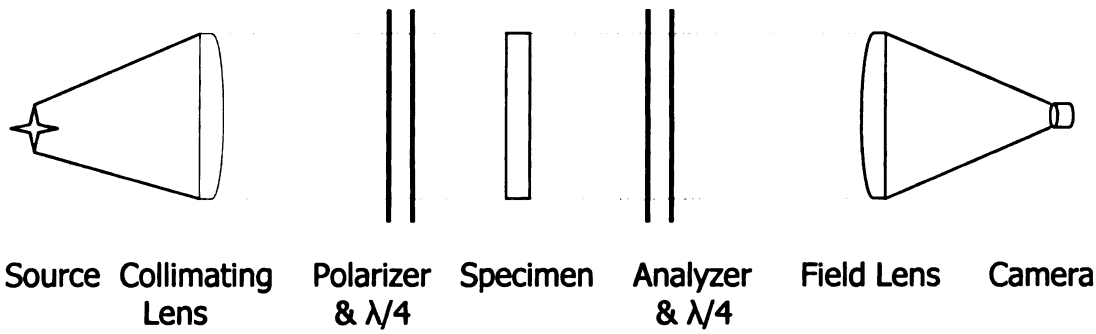

Figure 3.1 Schematic of a typical large field transmission polariscope.

The source is a sodium vapor discharge lamp, able to provide monochromatic light with a wave length of 589 nm. For some measurements a fluorescent light is used together with the sodium one in order to boost the intensity of the light for better fringe visibility.

The collimating and collecting devices are a pair of large field lenses of the same characteristics. They are elements which transform a polariscope into a large field polariscope. The collimating lens transforms the divergent light field into a collinear one, while the field lens converts the light into a convergent one. The convergent point is exactly the focus point of the lens. The collimating lens

is placed in front of the light source, with the source at its focus point. Another method can be used, to add a filter that will create a diffuse light. The field lens is placed after the second polarizer with the camera at its focal point. The two lenses used are 13 inches in diameter with a 39 inch focal length.

In our case, the polarizer, the analyzer, and the quarter-wave plates were embedded into the specimen, as shown in Figure 3.2. The polarizer and the retarding film were cut from commercially available sheet of Polaroid filter medium, type CP -01P (made by International Polarizer, Inc.). The quarter-wave plates have the role of converting the linear polarized light emerging from the polarizer into circularly polarized light. The circular polarization eliminates isoclinic fringes (loci of points of constant inclination of the principal axes of refraction).

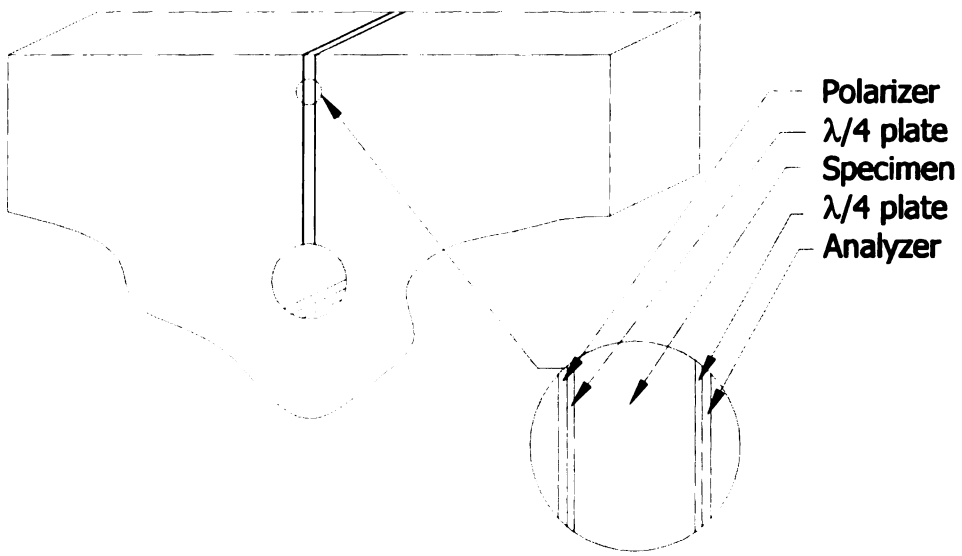

Figure 3.2. Embedded polariscope in a birefringent material plate.

Two cameras were used as recording devices. A COHU Solid State Camera with Coligon Zoom Lens 1:6.3 with f=95 – 205 mm, was connected to a computer and the pictures were captured using a virtual instrument (VI) program. The VI program was written under LabView, version 5.1, developed by National Instruments (National Instruments 2000). The second recording device was a digital camera, Sony Cyber-Shot P31. In both cases the camera aperture was placed so the distance from it to the field lens was equal to the focal length of the lens.

In addition to this setup a loading frame was used for loading the specimen in tension. Some of the calibration specimens were loaded in compression. The frame can be seen in Figures 3.3 and 3.4.

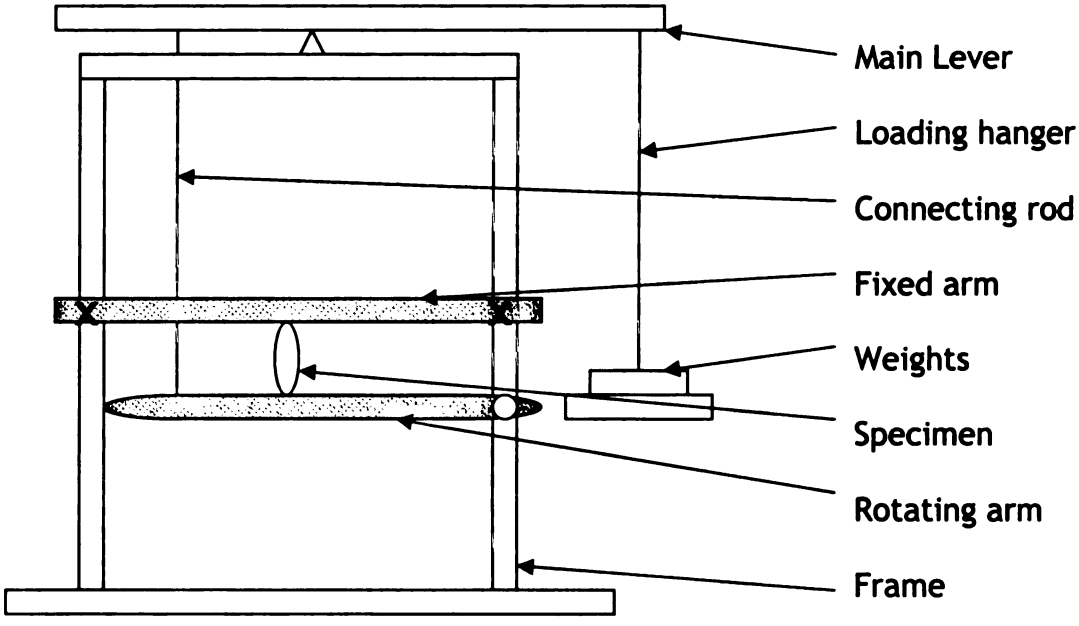

Figure 3.3. Loading frame – schematic.

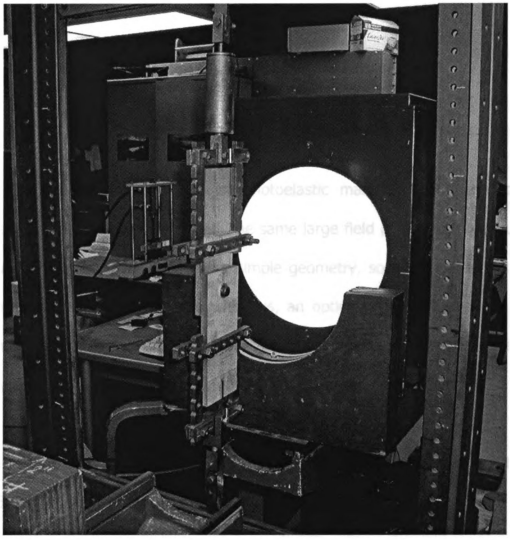

Figure 3.4. Loading frame – picture.

3.1.2. Calibration of the photoelastic material

In the process of calibration of photoelastic material, the stress-optic coefficient C_σ needs to be determined. The same large field polariscope in Figure 3.1 is used. The specimen used has a simple geometry, so the shear stress in every point can be computed, and with this, an optical stress analysis can be performed. The result will be a fringe pattern that, when used with the stress given by theoretical calculations, will provide the stress-optic coefficient C_σ.

The specimen is a block in compression and its dimensions are shown in the Figure 3.5:

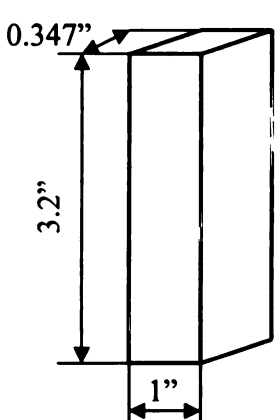

Figure 3.5. Calibration specimen – (dimensions are in inches).

Procedure

Step 1. Calibrate the polariscope (establishing the orientations of the axes of polarizers and λ/4 plates).

Step 2. Record isocromatic fringes for our specimen, both in dark field and light field.

Step 3. Measure the important dimensions related to specimen and loading the specimen.

Step 4. Plot the fringe order versus the stress difference along the axis of the specimen.

Step 5. Use the plot in part 4 to determine the stress-optic coefficient for the given material of the specimen.

The main lever ratio is 5:1 and the ratio of the lower lever is 1.57:1 (see Figure 3.3). The vector representation is shown in the Figure 3.6:

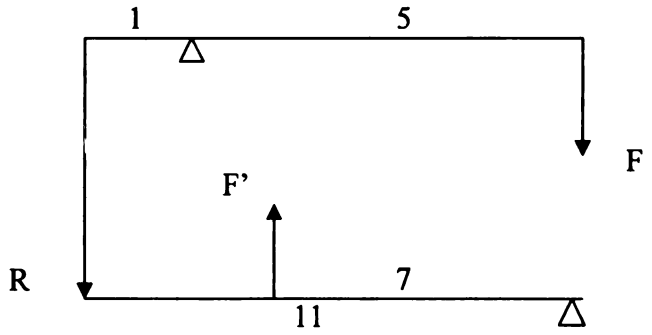

Figure 3.6. Vector representation of the loading forces.

The theoretical calculations for the rectangular block in uniaxial compression are (Ugural and Fenster 1995)

$$\sigma_1 = \frac{F'}{A} = \frac{F'}{\delta \cdot \ell} = \frac{\mathbf{7.85} \cdot F}{\mathbf{0.347} \cdot \mathbf{1}} = \mathbf{22.62} \cdot F \tag{3.6}$$

where F is the load applied to the hanger.

We assume σ_2 is close to 0, so it is negligible.

We know (Cloud 1995)

$$\sigma_1 - \sigma_2 = \frac{C_\sigma \cdot N}{\delta} \tag{3.7}$$

giving:

$$C_\sigma = \frac{\sigma_1 \cdot \delta}{N} = \frac{\mathbf{22.62} \cdot F \cdot \delta}{N} \tag{3.8}$$

where: δ is the thickness

N is the fringe order

Table 3.1 gives the experimental results:

		app. load	actual load	stress	fringes	Cσ
	[in]	[lbs]	[lbs]	[psi]		[psi in]
thickness	0.347	0	0	0	0.001	0.00
width	1	2	15.7	45.24	0.25	62.80
area	0.347	4	31.4	90.49	0.5	62.80
		6	47.1	135.73	0.8	58.88
		8	62.8	180.98	0.9	69.78
		10	78.5	226.22	1.1	71.36
		12	94.2	271.47	1.35	69.78
		14	109.9	316.71	1.55	70.90
		16	125.6	361.96	1.8	69.78
		18	141.3	407.20	2	70.65
			avg. Cσ		**67.41 psi in/fringe**	
			avg. Cσ		**11.8 MPa mm/fringe**	

Table 3.1. Determination of the stress-optic coefficient.

The graph in Figure 3.7 shows that the variation of stress (theoretically computed) with the fringe order is very close to linear. The stress optic coefficient determinations are in a tight range and the average result is

C_σ = 67.41 psi in /fringe

or

C_σ = 11.8 MPa mm /fringe

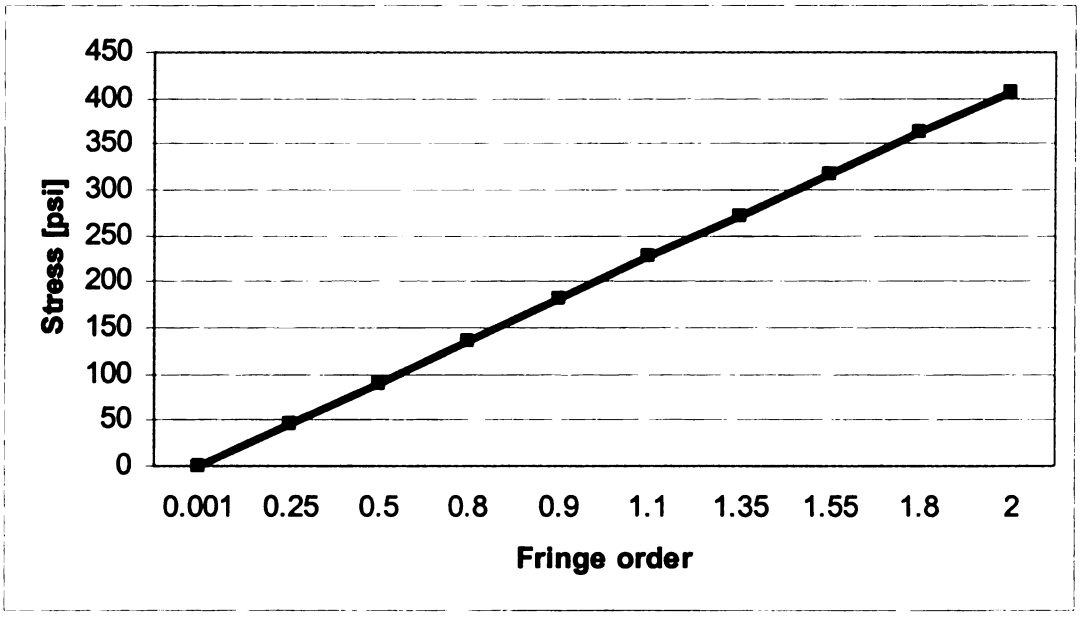

Figure 3.7. Correlation of the fringe order with stress.

For different loading states, fringes of different order form in the specimen and can be seen through the polariscope (Figures 3.8: a) – d)).

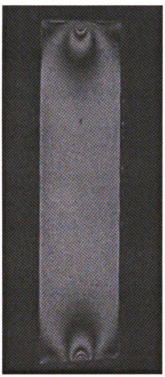

a)

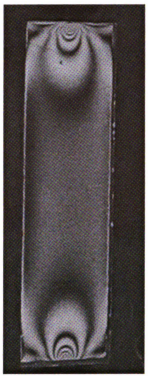

b)

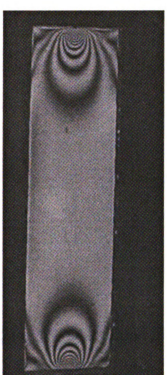

c)

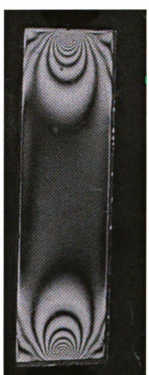

d)

Figure 3.8. Fringe pattern in the specimen under compression load: a) one and a half fringe; b) two fringes; c) two and a half fringes; d) three fringes (all counted in the middle of the specimen)

The second specimen investigated was the arch shown in Figure 3.9. The material is the same as for the calibration specimen. This new model will serve later on to verify the material properties that will be input to the finite element code.

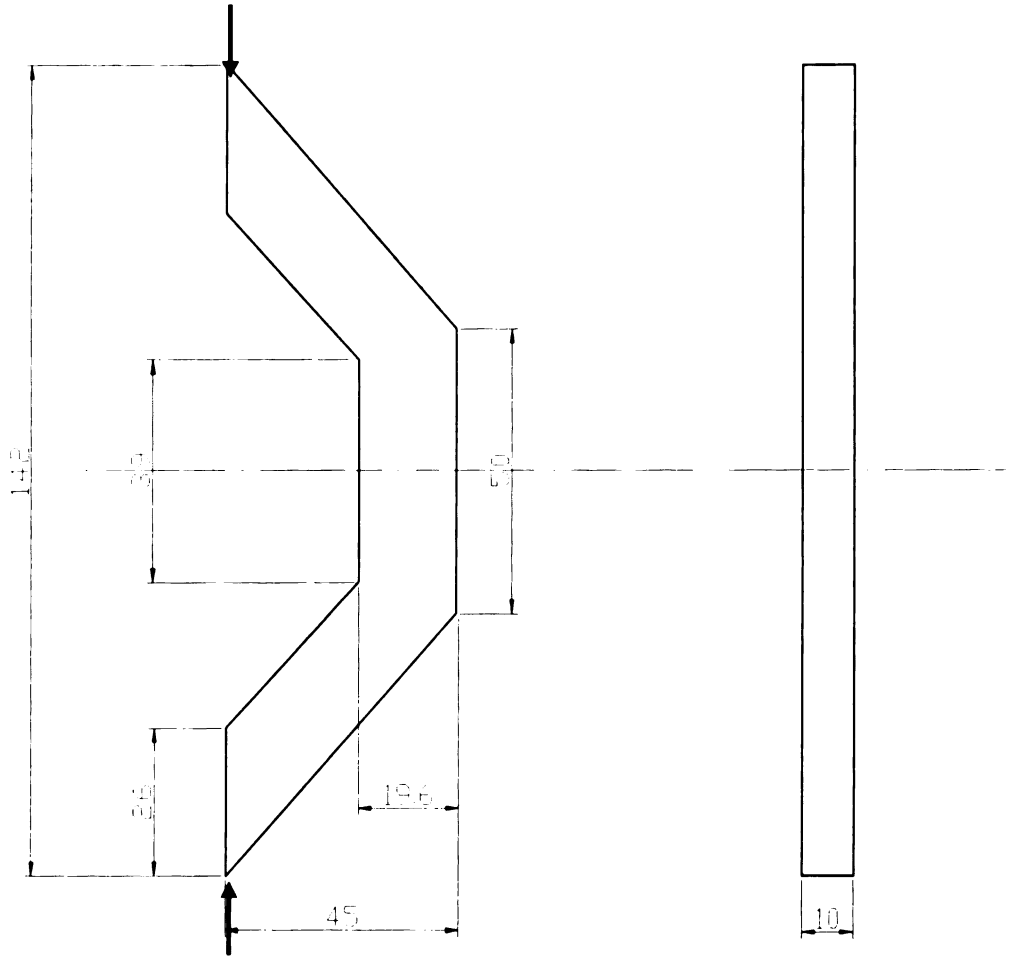

Figure 3.9. Description of the arch specimen (dimensions are in millimeters).

The arch was loaded in compression, the two loading points being at the two ends of the arch. The load applied to the specimen was 128.1N

The photoelasticity investigations provided the following result.

In point A in Figure 3.10, the shear stress has the value:

$$\sigma_1 - \sigma_2 = 2 \cdot \tau = \frac{6 \cdot 11.8}{10} = 7.08 \text{MPa} \qquad (3.9)$$

This result is based on the number of fringes in point A, 6, and on the formula (3.7).

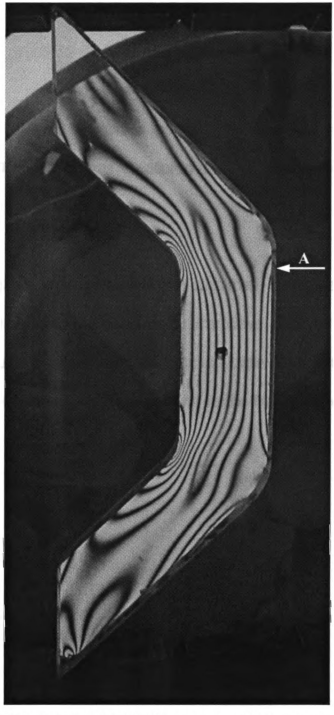

Figure 3.10. Shear stress distribution in an arch in compression.

3.2. STRAIN GAGE MEASUREMENTS

The second method of obtaining experimental results was direct strain measurements. The strain was measured in the bearing plane using three embedded resistance strain gages.

The strain gages were glued into the specimen, being placed between the body of the specimen and the polarizer-quarter wave plate foil (see Figure 3.2), that is on the surface of the embedded polariscope slice. The position of the strain gages in the bearing plane is according to the figure below.

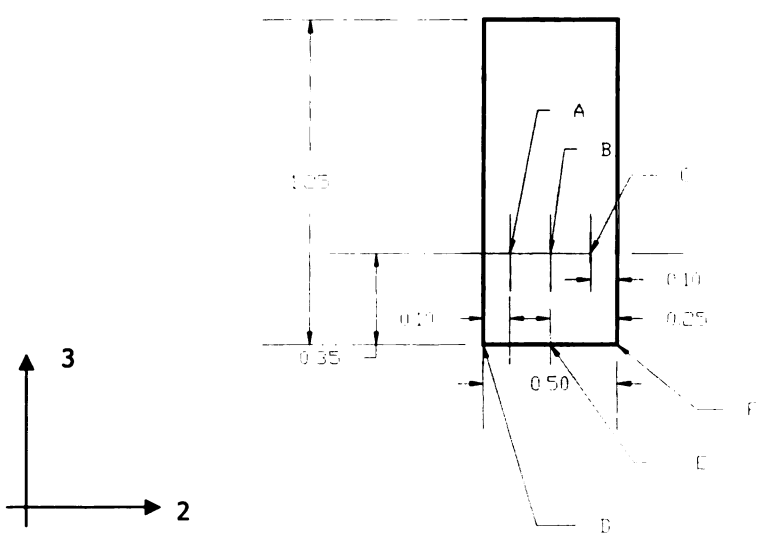

Figure 3.11. Position of the strain gages inside the bearing plane (all the dimensions are in inches).

The gages used were EP-08-015CK-120, with gage factor of 2.14 ± 0.3% and k_t = ±2.0 %, produced by Micro-Measurements Inc.

The slice in Figure 3.11 was cut out of the specimen plate and its position was in the bearing plane, as can be seen in Figure 3.12.

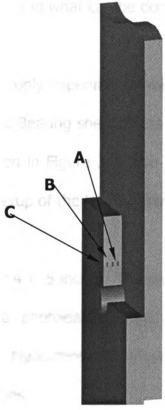

Figure 3.12. Position of the strain gages in the bearing plane of the photoelastic plate.

3.3. EXPERIMENTAL RESULTS

As described in the objectives, this research study tries to find out what and where the maximum shear stress in the bearing plane of a thick isotropic plate bolted to a metallic one is, and what can be done to lower this stress.

Photoelasticity is the only experimental method able to provide directly the values of the shear stress. Bearing shear stress in the isotropic plate was chosen to be studied, as described in Figure 3.2. The dimensions and the schematic of the joint, as well as the setup of the loading frame are presented next.

Both plates were 8 x 4 x .5 inches. The investigated plate is made of epoxy resin CR-39, which is a photoelastic sheet, type PSM-9, manufactured by Photoelastic Division of Measurements Group, Inc. The material has the following material properties:

E = 4.78 e5 psi

ν = 0.38

The supporting plate is made of aluminum, 2024-T4, with the following material properties:

E = 1.01e7 psi

ν = 0.34

The schematic of the joint is presented in the Figure 3.13.

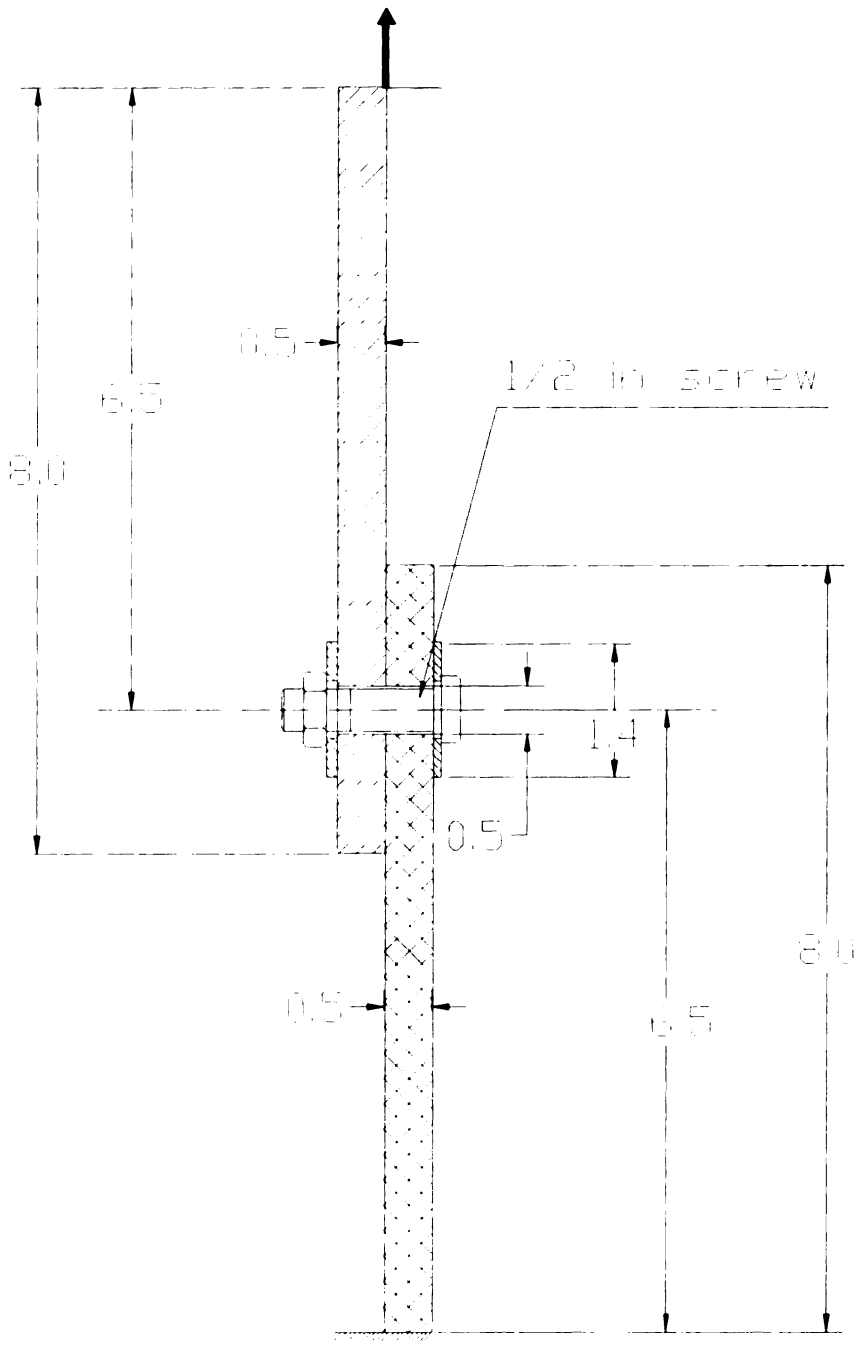

Figure 3.13. Single-lap bolted joint of composite and metallic plates (all the dimensions are in inches).

The loading frame and position of the plates in the loading frame are shown in Figure 3.14. The positions of the six measuring points (A, B, C are the positions of the strain gages, and D, E, F are the measuring points for photoelasticity measurements) are presented in Figure 3.15.

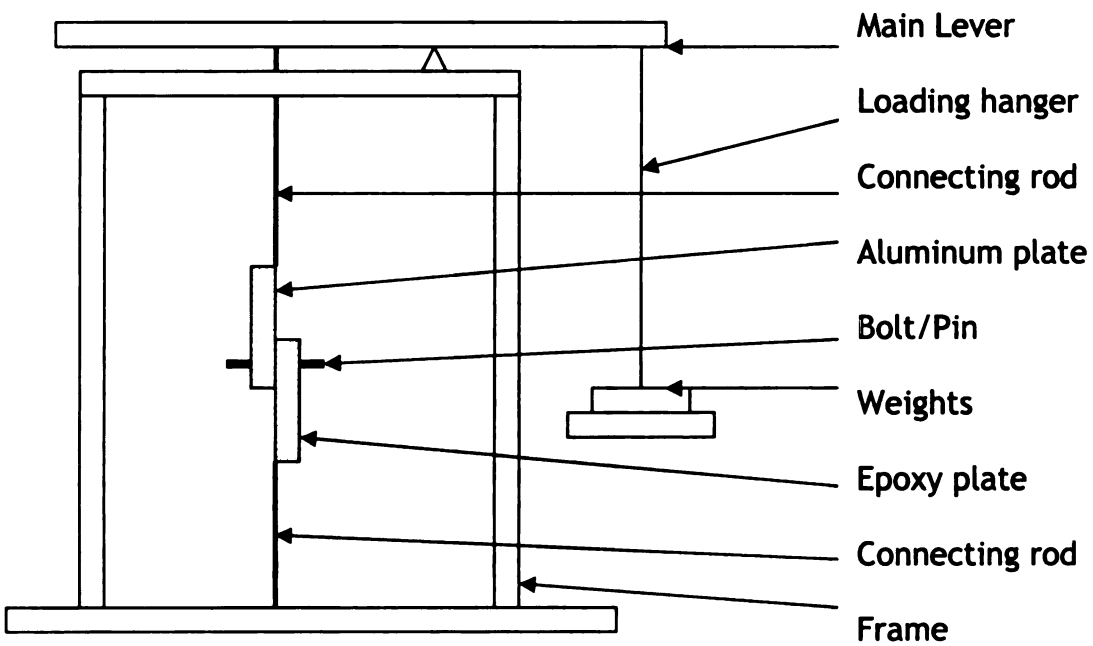

Figure 3.14. Position of the plates in the loading frame.

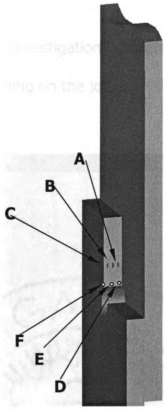

Figure 3.15. Position of the six measuring points.

3.3.1. Pin connection

In the first case studied, the two plates were connected by a half-inch diameter pin. The joint was loaded progressively up to 50lbs. Besides the fringe pattern recorded by the camera, some strain measurement were recorded from inside the tested plate (Measurements Group 1992). The positions of the strain gages can be seen in Figures 3.11 and 3.12.

The photoelasticity investigation delivered the fringe pattern shown in Figure 3.16, for 50lbs loading on the joint.

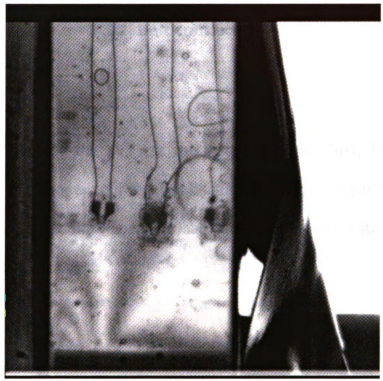

Figure 3.16. Shear stress fringe pattern in the bearing plane for a pin connection loaded at 50lbs.

It can be seen in the lower left corner, which is the point closest to the aluminum plate during loading and which has the highest shear stress, that there are 3.5 fringes (the white lines are full order fringes and the black ones are half order fringes). According to the formula (3.7), the shear stress is 700 psi with an uncertainty of 50 psi. The related, large uncertainty is a result of the fact that

only a single light-field fringe pattern can be obtained from the embedded polariscope method. Compensation methods to obtain fractional fringe order are not possible with the embedded polariscope method.

3.3.2. Bolt connection

In the second case the pin was replaced by a bolt. First, the bolt was tightened with a low torque, equivalent to finger tightening. The joint was loaded from 0lbs to 120lbs. For the maximum load, the shear stress distribution is as shown in Figure 3.17.

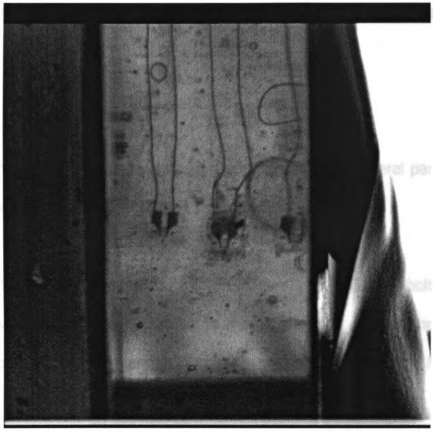

Figure 3.17. Shear stress fringe pattern in the bearing plane for a bolt connection loaded at 50lbs with a fastening load of 30lbs.

There are no high concentrations of stresses. The distribution is almost uniform. In the left corner there is only one fringe, while on the rest of the lower edge a half order fringe is visible. This means that the highest shear stress is in the same corner as for the pin connection; but, for a much higher load, the stress is only about 200 psi with the same uncertainty of 50 psi.

3.4 MEASUREMENTS OF CLAMPING FORCE AND FRICTION COEFFICIENTS

In order to create the finite element model of this joint, several parameters of the joint and the material need to be measured.

The first thing is to convert the applied torque on the nut and bolt into an axial force, which in turn will be applied to the modeled nut and bolt head. The "Standard book of fastening and joining" (Parmley 1977) gives the following formula:

$$T = K \cdot D \cdot P \tag{3.10}$$

where T is installation torque, lbs-in.

K is the torque coefficient

D is the nominal bolt diameter, in

P is the clamp load objective, lbs

To verify this formula a strain gaged bolt, manufactured by Karen Corp., was used (Figure 3.18). The calibration of the bolt gave a relation between the

load applied to the bolt and the strain measured by the strain gage. The results of the calibration are in the table 3.2.

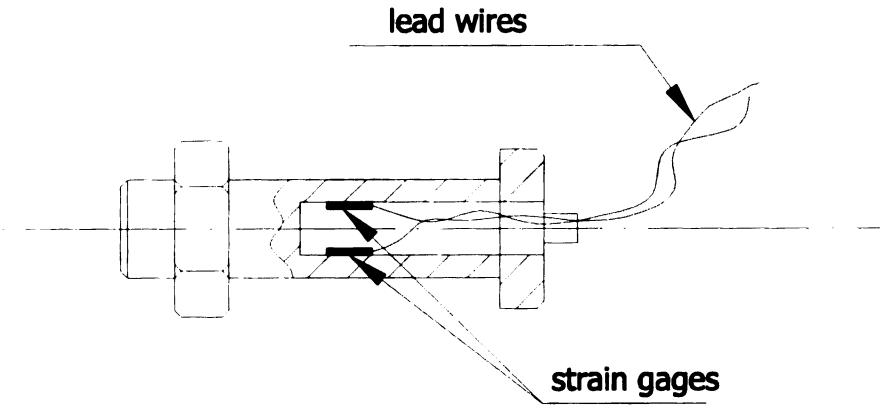

Figure 3.18. Strain measuring bolt.

Load (lbs)	Strain (με)
40	2
50	7
75	17
100	27
120	36
140	44
160	52
180	61
210	71

Table 3.2. Calibration of strain measuring bolt.

These data are plotted in Figure 3.19, and the relation between the strain readings and the force applied can be deduced. The relation is

$$L = 2.4007\,\varepsilon + 35.365 \qquad (3.11)$$

where L is the load in-lbs

and ε is the strain in με.

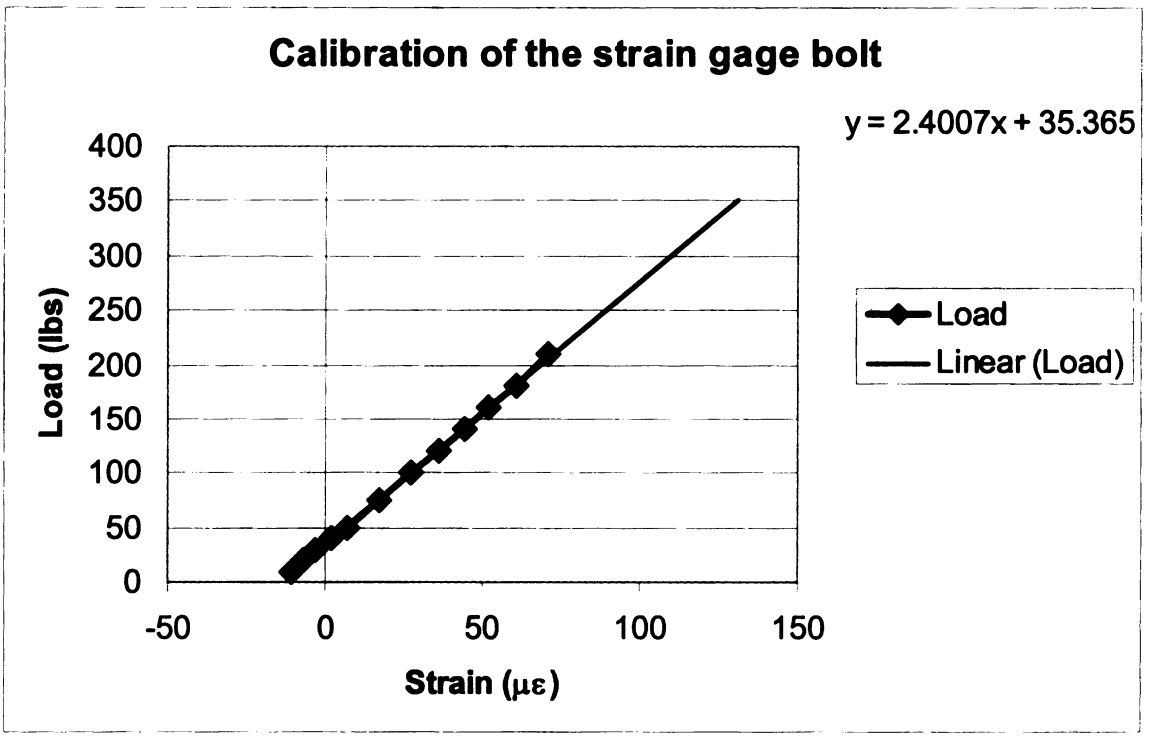

Figure 3.19. Calibration of the strain gage bolt.

The curve was extrapolated up to 350lbs for future measurements.

For a 25 in-lbs torque, a strain of about 65 με was measured in the bolt, and that would be converted into 190 lbs normal force. For 40 in-lbs torque, 114 με were measured, which in turn, converted into 300 lbs normal force.

Next, the friction coefficient between all the parts of the joint in contact needed to be measured. The simplest way to measure it is the tangent of the angle at which one object starts sliding on the other (see Figure 3.20).

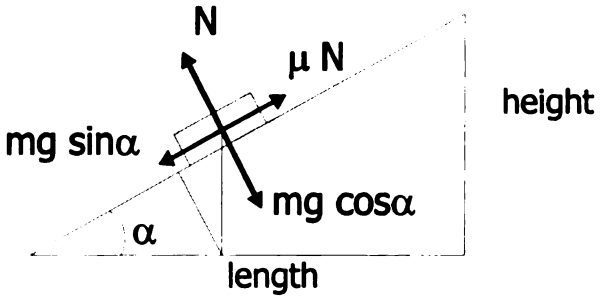

Figure 3.20. Friction coefficient measuring scheme.

In tables 3.3 to 3.5 are the measured friction coefficients between different materials involved in the single-lap joint.

CR-39 and Aluminum		
Height [mm]	**Length** [mm]	**Friction coefficient**
44.8	137.4	0.326
44.5	100	0.445
46.5	100	0.465
38.5	100	0.385
39.6	100	0.396
43	100	0.430
38.4	100	0.384
41.9	100	0.419
	Average	**0.406**

Table 3.3. Determination of friction coefficient between CR-39 and aluminum.

Aluminum and Aluminum		
Height [mm]	**Length** [mm]	**Friction coefficient**
49.4	100	0.494
48.2	100	0.482
49.5	100	0.495
	Average	**0.490**

Table 3.4. Determination of friction coefficient between aluminum and aluminum.

Steel and CR-39		
Height [mm]	**Length** [mm]	**Friction coefficient**
47.4	100	0.474
49.1	100	0.491
48.4	100	0.484
	Average	**0.483**

Table 3.5. Determination of friction coefficient between CR-39 and steel.

Chapter 4

FINITE ELEMENT ANALYSIS

Some researchers consider that finite element analysis (FEA) is merely an alternative approach to solving the governing equations of a structural problem (Matthews, Davies et al. 2000). Given the improved performances of the new generation of computers and the development of the new commercial FEA codes, FEA has become a very powerful tool in designing and investigating mechanical components. Powerful, because it saves time and money and the results, even if they are not a hundred percent accurate, give us a good idea of the behavior of the component.

A brief definition of the finite element method would sound like this: The finite element method is a numerical analysis technique for obtaining approximate solutions to a wide variety of engineering problems. This technique works by reducing a real problem which has an infinite number of unknowns to a finite number of unknowns by dividing the solution region into elements and by expressing the unknown field variable in terms of assumed approximating functions within each element (Huebner, Dewhirst et al. 2001).

All structural analysis can be summarized by four separate, but linked conditions to be modeled and satisfied, as illustrated in Figure 4.1.

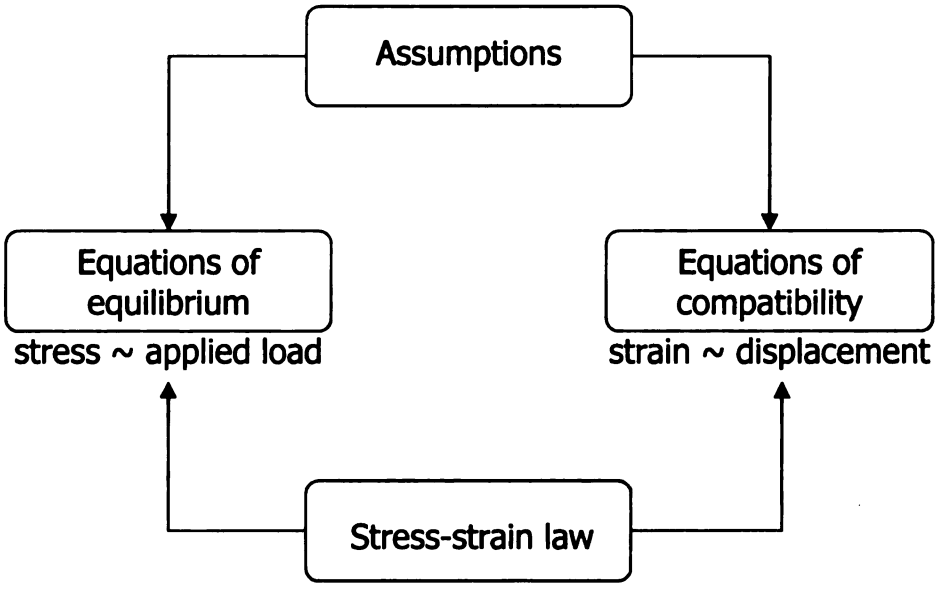

Figure 4.1. Conditions of the finite element analysis.

An important goal of this research was to develop a finite element model that could be used to achieve a better understanding of the behavior of the thick single-lap joint. Later on, the model can be employed to predict the performance of some alternative joint designs. That would save money and time by reducing the amount of trial and error associated with the experimental work, and would suggest directions to follow. Commercial FEA packages are effective enough that they can be used with confidence as predictive tools, provided that the correct data are introduced: geometry, material properties, force and displacement boundary conditions, contacts, etc.

4.1. DESCRIPTION OF THE FEA MODEL

The numerical study of the single-lap joint was done using the explicit finite element code ABAQUS 6.2. The preprocessor used to build the finite element model was HyperMesh 5.0 and the postprocessor used to view the results was ABAQUS/Viewer 6.3-1. In this chapter, some important information regarding the building of the model as well as issues affecting the accuracy of the results will be presented.

HyperMesh is a product of Altair Computing Inc. HyperMesh is a full-featured, linear and nonlinear pre- and post-processor. In addition, HyperMesh also lends itself well as a finite element model editor to supplement larger pre- and post- processing systems (Altair Computing 2001).

ABAQUS/Standard and ABAQUS /Viewer are products of Hibbitt Karlsson & Sorensen. ABAQUS is a suite of powerful engineering simulation programs, based on the finite element method, that can solve problems ranging from relatively simple linear analyses to the most challenging nonlinear simulations (Hibbitt Karlsson & Sorensen 1998). ABAQUS/Standard is a general-purpose analysis

module that can solve a wide range of linear and nonlinear problems involving static, dynamic, thermal and electrical response of components.

The first model created was the arch studied in the photoelasticity section, chapter 3.1. This model was used to verify that the material properties input in the model are correct. The same material with the same properties will be used for the single-lap joint of thick composite and metallic material.

The model can be seen in Figure 4.2 and is composed of 210 brick elements C3D8I, with one end simply supported and nodal forces applied at the other end.

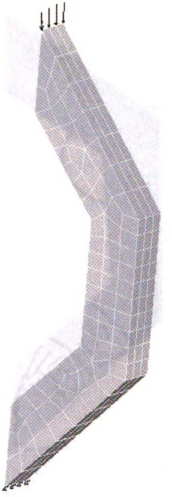

Figure 4.2. Typical mesh of an arch in compression.

The results can be seen in Figure 4.3 and show that in point A (see Figure 3.13) the shear stress has the value 3.4 MPa. The error between the numerical result and the result of the experimental study described in chapter 3 is found as follows:

τ_{exp} = 3.54 MPa (from equation 2.4)

τ_{FEM} = 3.4 MPa

$$\varepsilon = \frac{\tau_{exp} - \tau_{FEM}}{\tau_{exp}} = \frac{\mathbf{3.54 - 3.4}}{\mathbf{3.54}} = \mathbf{0.039} = \mathbf{3.9\%} \qquad (4.1)$$

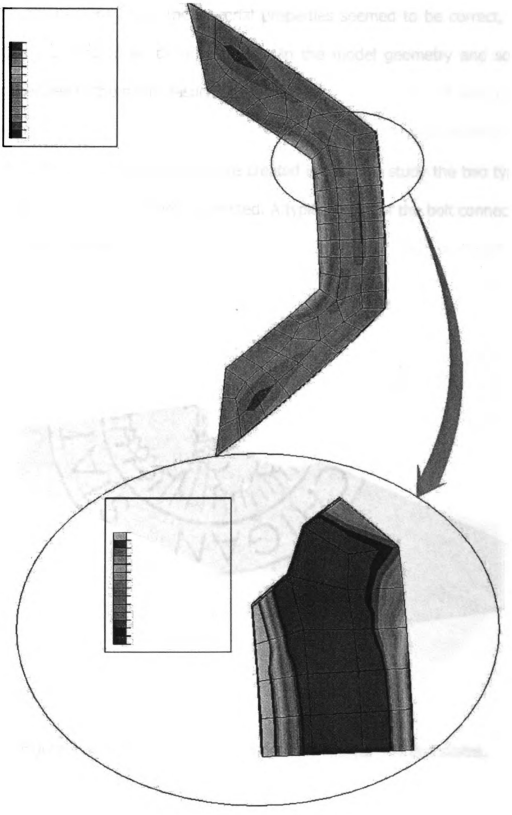

Figure 4.3. Shear stress (τ_{12}) map of an arch in compression (in MPa).

The assumptions about the material properties seemed to be correct, the errors being generated by the inaccuracies in the model geometry and some errors generated in the photoelasticity experiment.

Several finite element models were created in order to study the two types of joints: pin connected and bolt connected. A typical mesh of the bolt connected joint is shown in Figure 4.4.

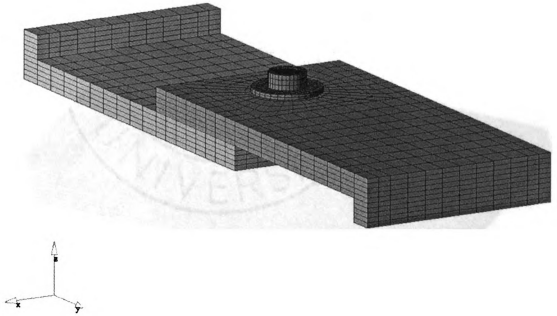

Figure 4.4. Typical mesh of a single-lap bolted joint of two plates.

A typical mesh of a plate is shown in Figure 4.5. The mesh is divided into two regions: a square corresponding to the overlap area with a finer mesh surrounding the bolt hole and a rectangle with a coarser mesh for the remainder. The plates have an offset strip at the ends so the loading plane is coincident with the contact surface. The square is in turn divided into two sub-parts: a cylindrical part under the washers and the rest of the square. Thirty-two elements were used around the hole. The same number of elements was used to model the circumference of the bolt and the bolt head. All the elements used for modeling the geometry were C3D8I, eight-node, solid elements.

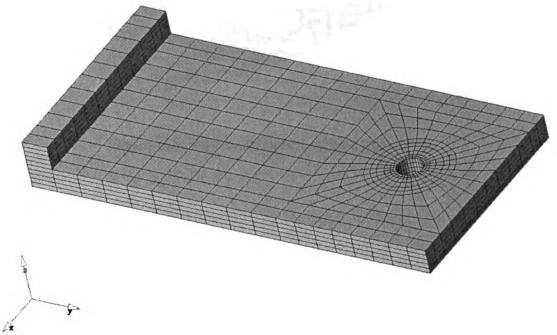

Figure 4.5. Typical mesh of a single plate.

The bolt, bolt head and washer were modeled as a single object to limit the number of contact surfaces in the model. The nut was modeled together with the second washer and a contact pair was created between the inside of the washer and the outside of the bolt. A high friction coefficient, 0.49, was applied to these surfaces, in order to simulate the effect of the thread. Figures 4.6 and 4.7 show the nut-washer component and the whole fastening assembly.

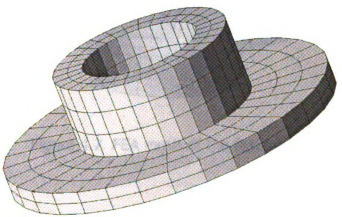

Figure 4.6. FEA mesh of the nut-washer unit.

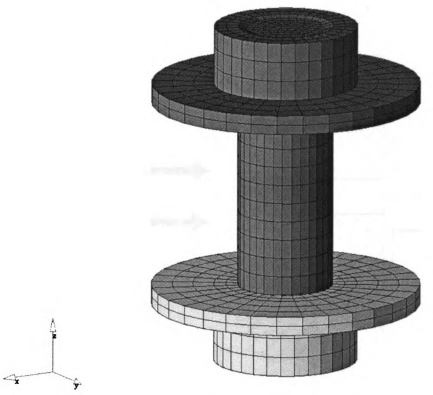

Figure 4.7. FEA mesh of the fastening units.

The model was based on idealization of the fastening system (Speck 1997). After establishing the fastening loads (see Figure 4.8), the free body diagrams can be drawn, Figure 4.9 and 4.10. The torque applied to the bolt and nut was converted into a compressive load applied to the bolt-head and nut.

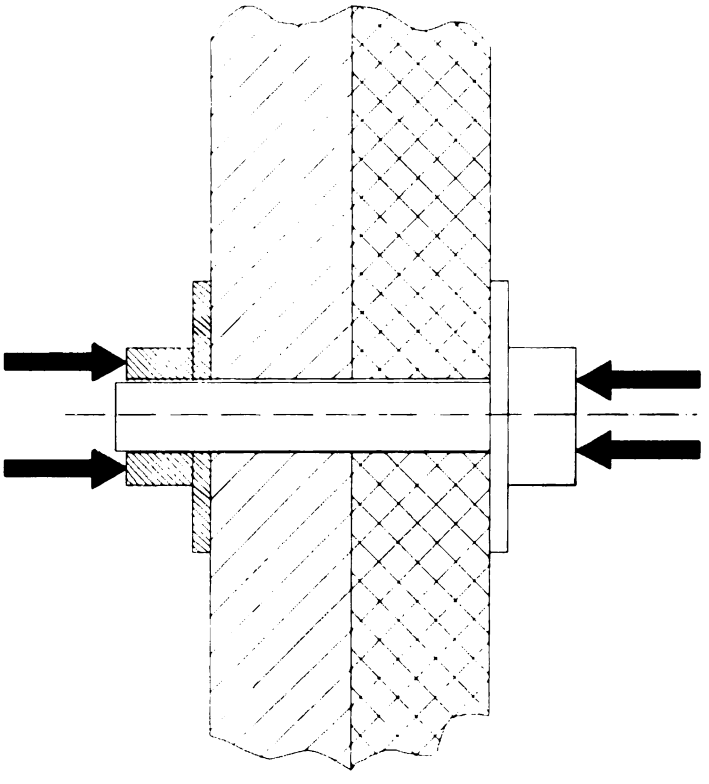

Figure 4.8. Fastening forces on the joint.

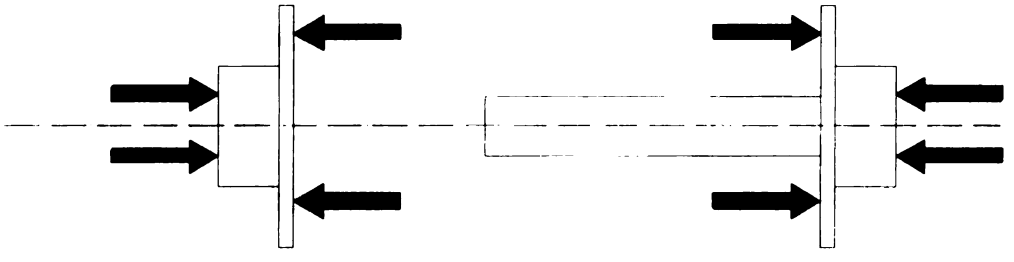

Figure 4.9. Free body diagram of the bolt-washer and nut-washer.

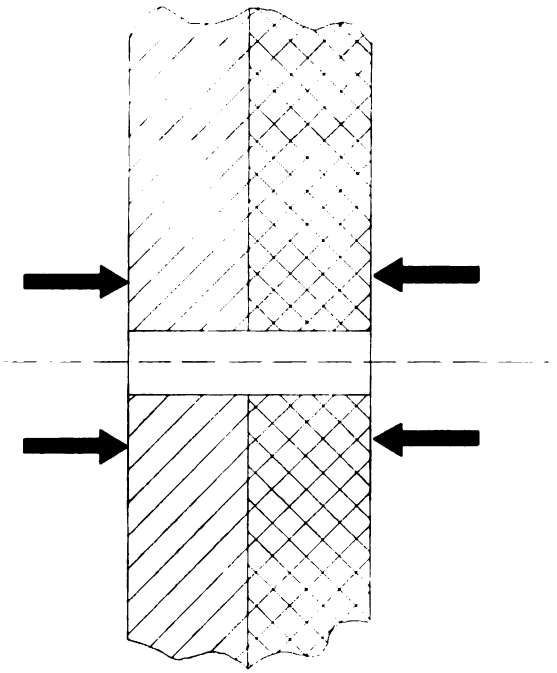

Figure 4.10. Free body diagram of the plates.

Contact between the aluminum and resin, the aluminum and the steel bolt-washer, the plates and the bolt, and the resin and nut-washer was modeled using the contact pair approach in ABAQUS. This approach is based on the master-slave concept, and the contact problem was solved using the Lagrange multiplier method. The contact pairs are defined from surfaces which in turn are defined from free element faces. The contact pair approach was selected for its simplicity in the definition of the possible contacts. Since sliding between parts was expected to be small, the "small sliding" option was used in all analyses. This option implied that possible contact between master and slave nodes is defined at the beginning of the analysis and is not redefined during the analysis. This assumption works if the deformations are small enough and if the nodes

remain in contact throughout analysis. The contact surfaces used in the model are shown in Figure 4.11 Two different surface interaction properties were created for applying two friction coefficients to the contact pairs.

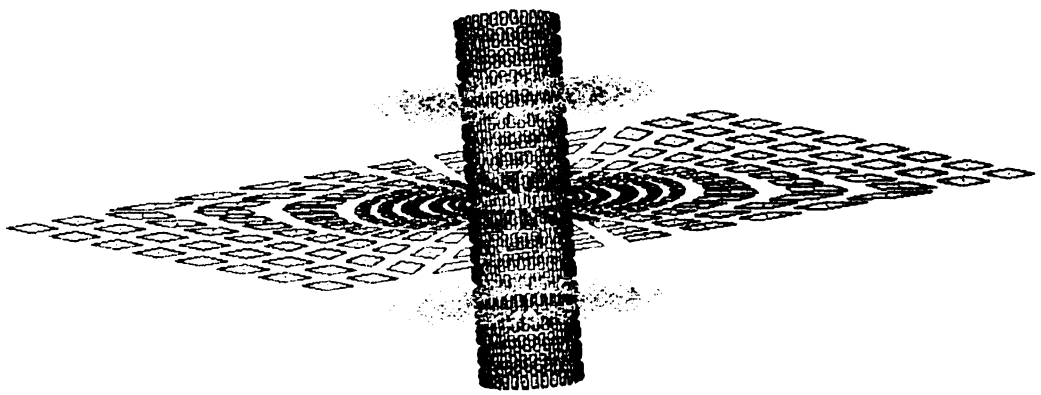

Figure 4.11. Contact pairs involved in a single-lap bolted joint.

A complete finite element model of a single-lap bolted joint, with the boundary conditions and loading applied, can be seen in Figure 4.12. The resin plate was fixed on one direction at one end. On the nodes at the end of the aluminum plate, a static force was applied as a concentrated load. The pretension load in the fastener (for the bolt connection) was applied in a separate loading step. The clamping force was simulated by a constant distributed nodal load applied on the bolt head and nut in every point of their volume.

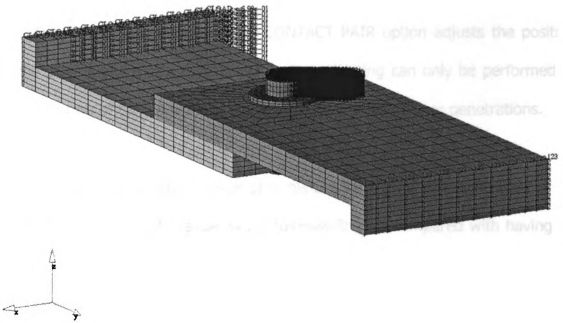

Figure 4.12. Complete FEA model of two bolt connected plates.

4.2. PARAMETERS AFFECTING THE FEA ACCURACY

During the development of the FEA code, some important parameters were encountered that were affecting the accuracy of the model by a significant amount.

4.2.1 Adjustment of the contact pair

The ADJUST parameter on the CONTACT PAIR option adjusts the position of the slave surface of a contact point. The adjusting can only be performed at the beginning of the simulation, and it eliminates small gaps or penetrations.

By choosing an adjust value of a hundredth part of the dimension of an element, the result will change by approximately 30% compared with having no adjust. Since the model was created ideally and the distance between nodes belonging to the master and slave surfaces was zero, and taking into consideration that the movement of the parts with respect to each other is insignificant, we chose zero adjustment value for all the contact pairs.

4.2.2 Geometrical effects

The geometry of the plates is created from the dimension and the size of the real plates and there is not much room for alternate models. But for the washer-bolt and washer-nut units, two models were created. In the first, in which the nut and washer were just a cylinder (Figure 4.13) The second one, more realistic, is the one used in the final model (see Figure 4.6).

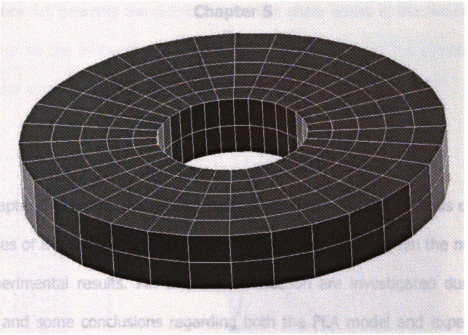

Figure 4.13. Initial design of the nut-washer unit.

The difference was that, with this original unit there was a high stress concentration in the plates in the region of the outer diameter of the nut, which does not appear on any experimental result. The second model was chosen for its accurate response compared to the experimental results.

The same effect was noticed when the force was applied on the washers, instead of applying it only on the nut and bolt head.

Chapter 5

RESULTS

Chapter 5 presents the results obtained by finite element analysis of all the load cases of the single-lap bolted joint, and comparisons between the numerical and experimental results. Pin and bolt connection are investigated during this chapter and some conclusions regarding both the FEA model and experimental results will be drawn.

5.1. PIN CONNECTION

In the following section the results for pin connection are presented. As mentioned before, several results were recorded by the strain gages placed in points A, B and C (Figure 3.15) for different loads. Experimental stress data were also recorded by a method of 3D photoelasticity. The results obtained through experimental methods are compared with the numerical ones, obtained through finite element analysis. The FEA gives the advantage of obtaining results in any point of the analyzed part subject to assumptions made about material properties, contact friction and others.

Figure 5.1 presents the distribution of the shear stress in the bearing plane (the same as the embedded polariscope). Figure 5.2 shows the distribution of the normal strain in the 2 direction for 50 lbs load.

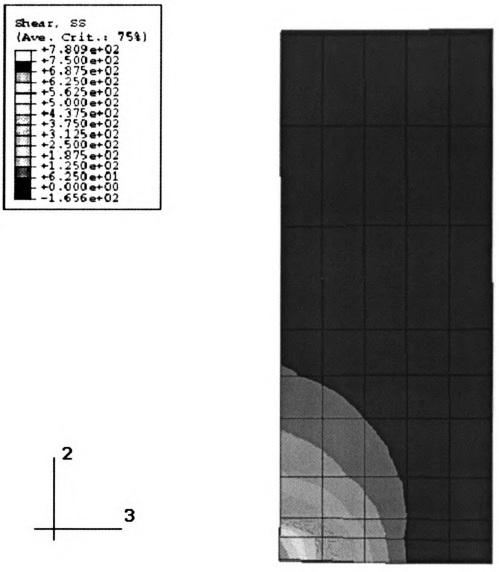

Figure 5.1 Distribution of shear stresses in the bearing plane of the CR-39 plate for pin connection and 50 lbs load on the joint (results are in psi).

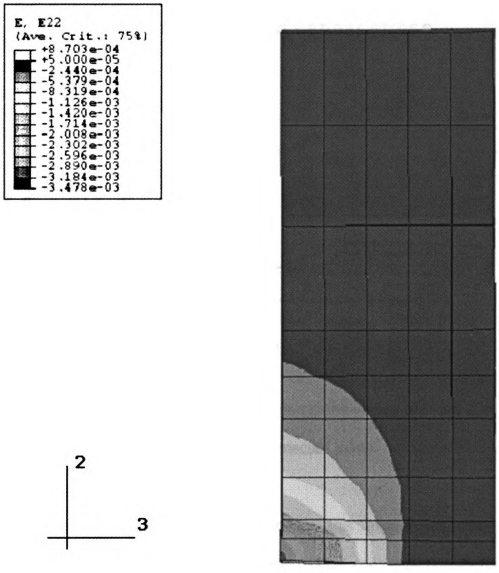

Figure 5.2 Distribution of normal strain on 2-direction in the bearing plane of the CR-39 plate (results are in $\mu\varepsilon$) for pin connection and 50 lbs load on the joint.

The map of the shear stress obtained numerically matches very well the experimental results obtained by photoelasticity. Figure 5.3 and 5.4 show the comparison between the stresses and strains, respectively.

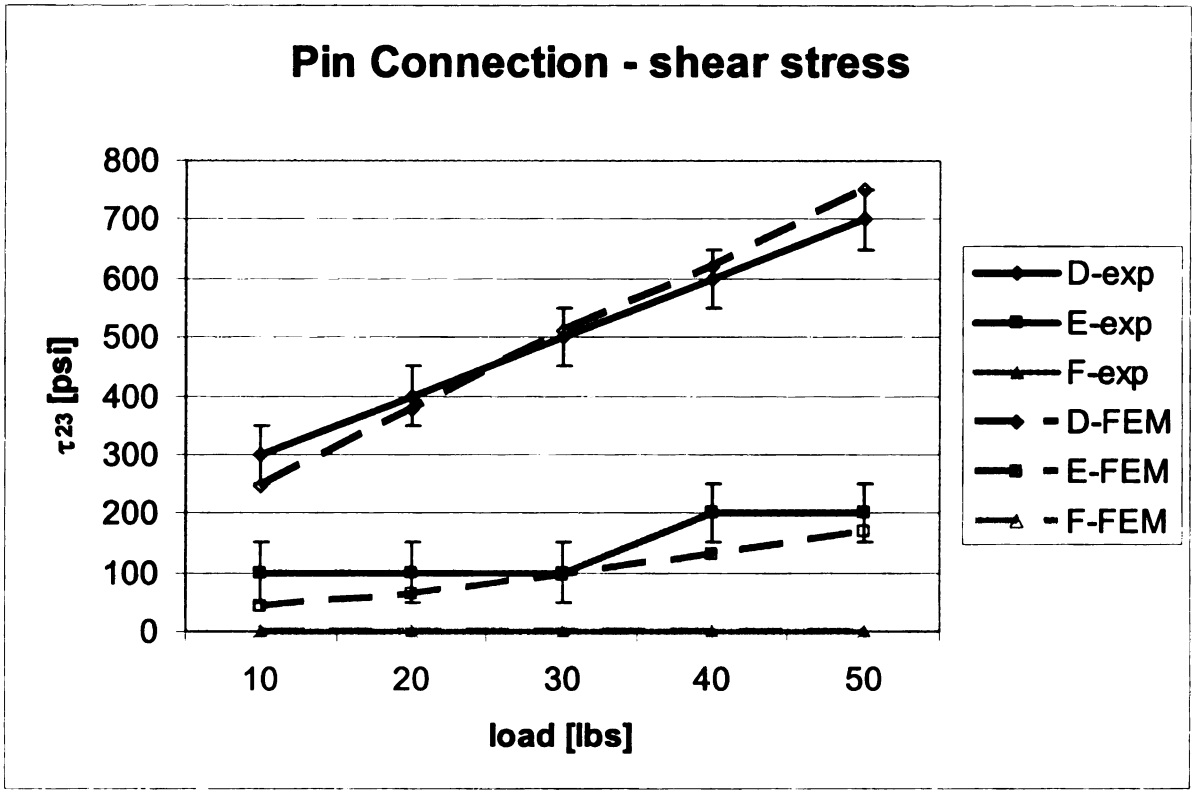

Figure 5.3 Shear stress in the bearing plane versus the load applied to the joint (pin connected joint).

The photoelasticity method used for this experiment, the embedded polariscope, has one major disadvantage. Optical compensation methods cannot be applied in order to obtain an exact value of the difference in relative refractive indices. That is why there is a ±50psi error bar, equivalent to one half fringe order, on all the values obtained from photoelasticity.

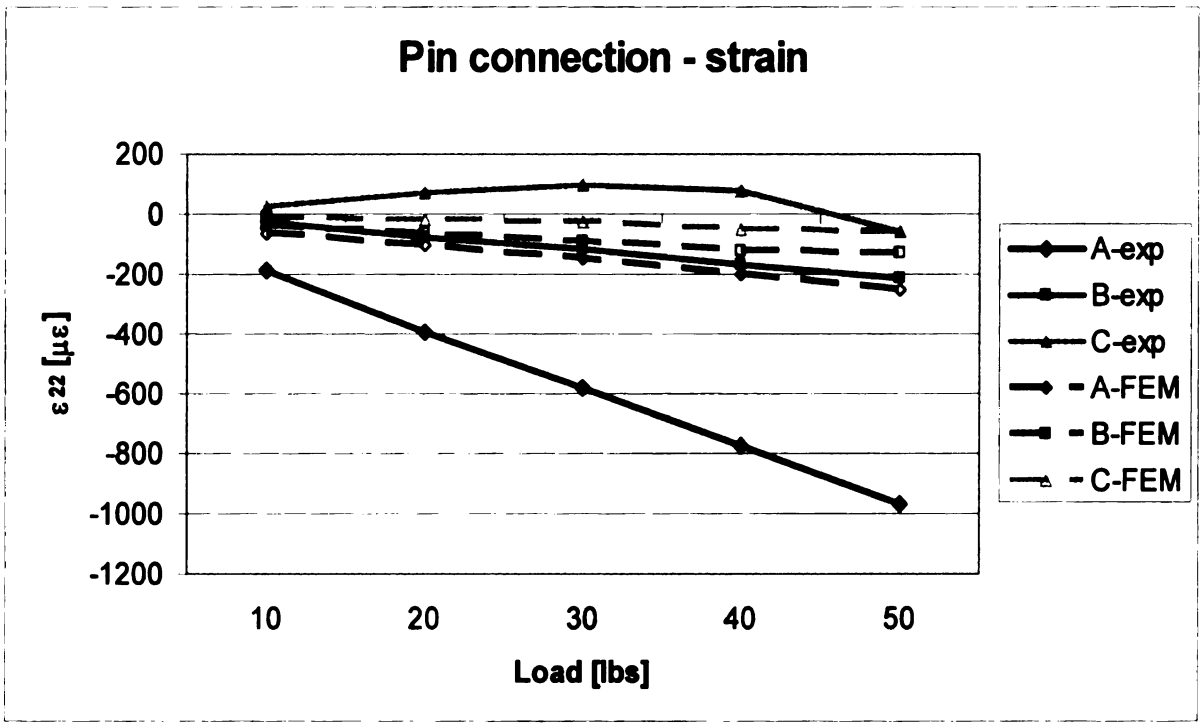

Figure 5.4 Normal strain in the bearing plane versus the load applied to the joint (pin connected joint).

As can be seen from the graph in Figure 5.4 the numerical results match very closely the experimental ones for strain gages 2 and 3, that is points B and C. At point A, the experiment provides results with much higher magnitudes than FEA. Possible causes of this error are described in detail in section 6.2.

The maximum stress on the bearing plane is where the resin plate meets the aluminum plate and the pin. This is the predicted result since the two plates are moving with respect to each other, movement which causes the tilting of the pin. The new position of the pin changes its contact with the plate from a line to a point, the point of maximum stress. By applying a constraint in the movement

of the pin, a decrease in the value of the maximum stress is expected. This constraint can be achieved by replacing the pin with a bolt and applying a torque on the bolt and nut.

5.2. BOLT CONNECTION

The same results as for pin connection are now presented for the bolt connection. The pin was replaced by a bolt, on which a torque of about 4 in-lbs was applied (approximately the value of the torque obtained by finger tightening). In Figures 5.5 and 5.6 the shear stress results obtained by FEA for 120 lbs load and normal strain for 140 lbs load are presented.

Figures 5.7 and 5.8 compare the FEA results with those obtained from photoelasticity and strain gage experiments.

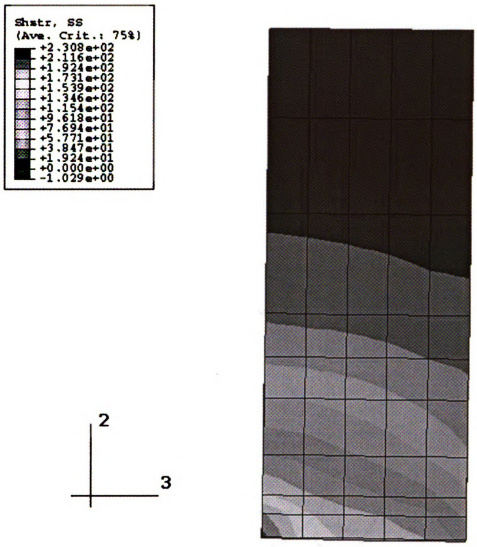

Figure 5.5 Distribution of shear stresses in the bearing plane of the resin plate for 4 in-lbs torque on the bold and 120 lbs load on the joint (results are in psi).

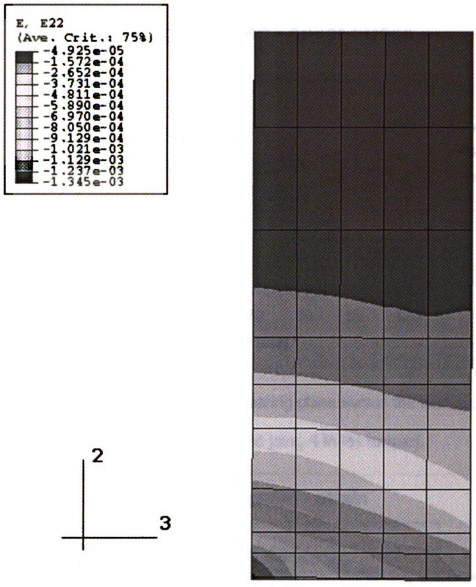

Figure 5.6 Distribution of normal strain in 2-direction in the bearing plane of the resin plate for 4 in-lbs torque on the bold and 140 lbs load on the joint (results are in $\mu\varepsilon$).

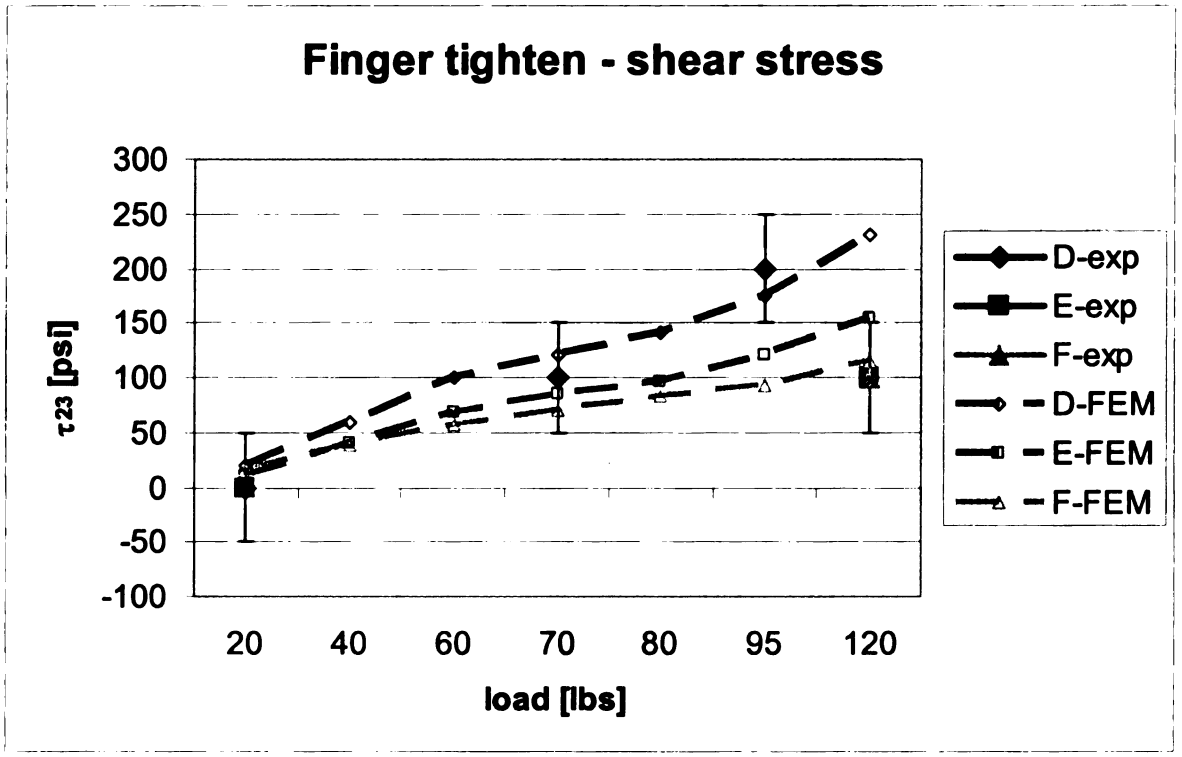

Figure 5.7 Shear stress in the bearing plane versus the load applied to the joint (bolt connected joint, 4 in-lbs torque).

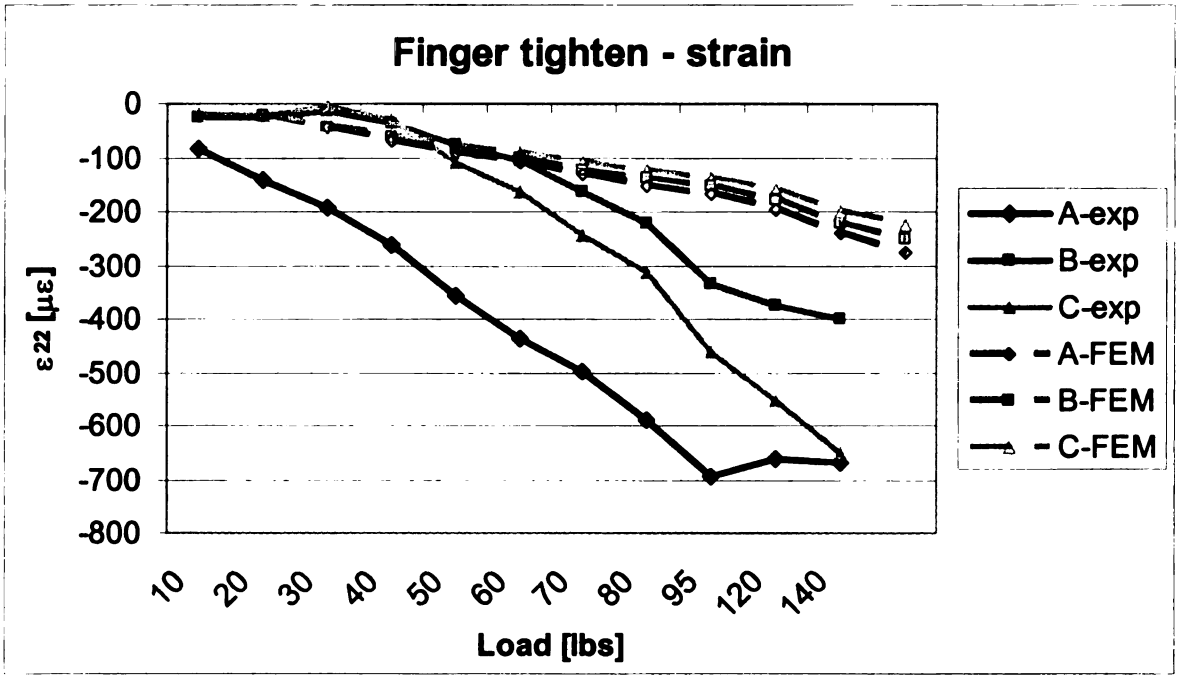

Figure 5.8 Normal strain in the bearing plane versus the load applied to the joint (bolt connected joint, 4 in-lbs torque).

The difference in stress values obtained by FEA and photoelasticity investigations is under 15 %. That is a reasonable result, taking into consideration that the photoelasticity provides us results with a margin of error of 50 psi. As for the pin connection, the strain results are not that close, especially for strain gage number one. The values obtained numerically and experimentally are close for small loads, up to 70 lbs.

Examination of Figures 5.1 and 5.5 leads to two general conclusions. The magnitudes of stresses are much lower for bolt connection than for pin connection. That means that friction between the two plates is taking over some of the load in the joint. The second conclusion is that the fringe pattern has changed, the stress being more uniformly distributed over the thickness of the plate, which was the desired result.

The bolt was tightened to two different torque levels. The first was 25 in-lbs, which was converted to normal loading on the bolt head and nut of 190 lbs. The second torque was 40 in-lbs, which was converted to 300 lbs.

In Figures 5.9 and 5.10 a comparison between the FEA results and the experimental ones is presented for the bolt connection with a torque of 25 in-lbs applied on the bolt. Figure 5.9 displays the results of the shear stress in the bearing plane, while Figure 5.10 shows strain values in the same plane.

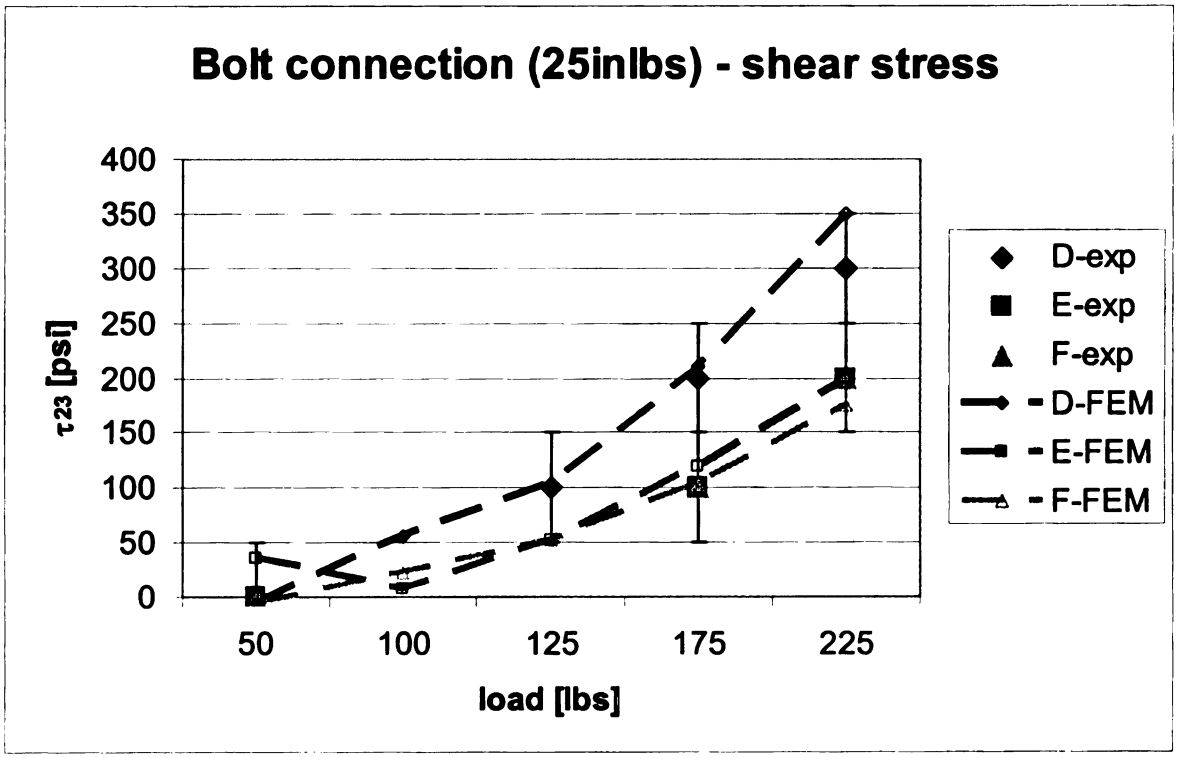

Figure 5.9 Shear stress in the bearing plane versus the load applied to the joint (bolt connected joint, 25 in-lbs torque).

The shear stresses have very similar values for experimental and numerical results in all three points measured. For the point of maximum stress, FEA predicts a higher value than the experiment, which can only lead to a safety factor in the design of the product.

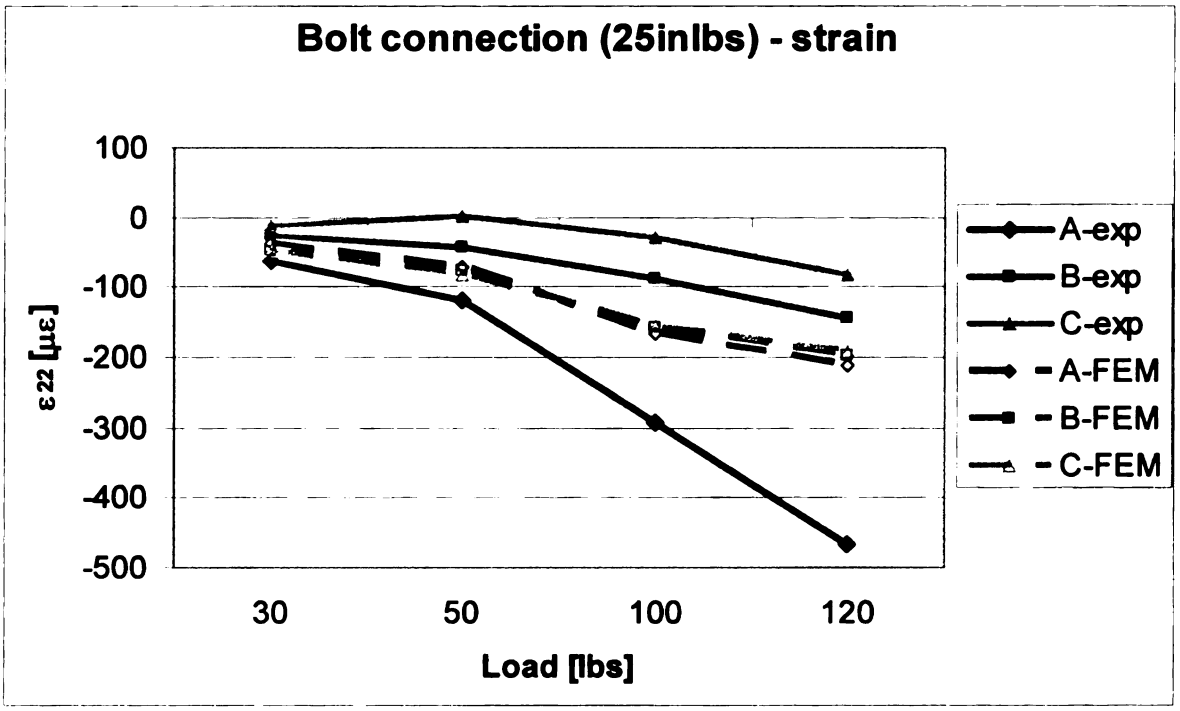

Figure 5.10 Normal strain in the bearing plane versus the load applied to the joint (bolt connected joint 25 in-lbs torque).

The strain results provided by experiment and finite element modeling appear to be similar for the middle point only. The causes of errors have both experimental and numerical provenance: delamination of the investigated slice from the plate, which causes false readings from the strain gages, presence of an air bubble next to the third strain gage and application of the force on the bolt on the same direction through all the steps of the simulation. A more extended discussion about these errors can be founded in section 6.2.

The same comparisons as for 25 in-lbs torque are displayed in Figures 5.11 and 5.12, but for 40 in-lbs torque.

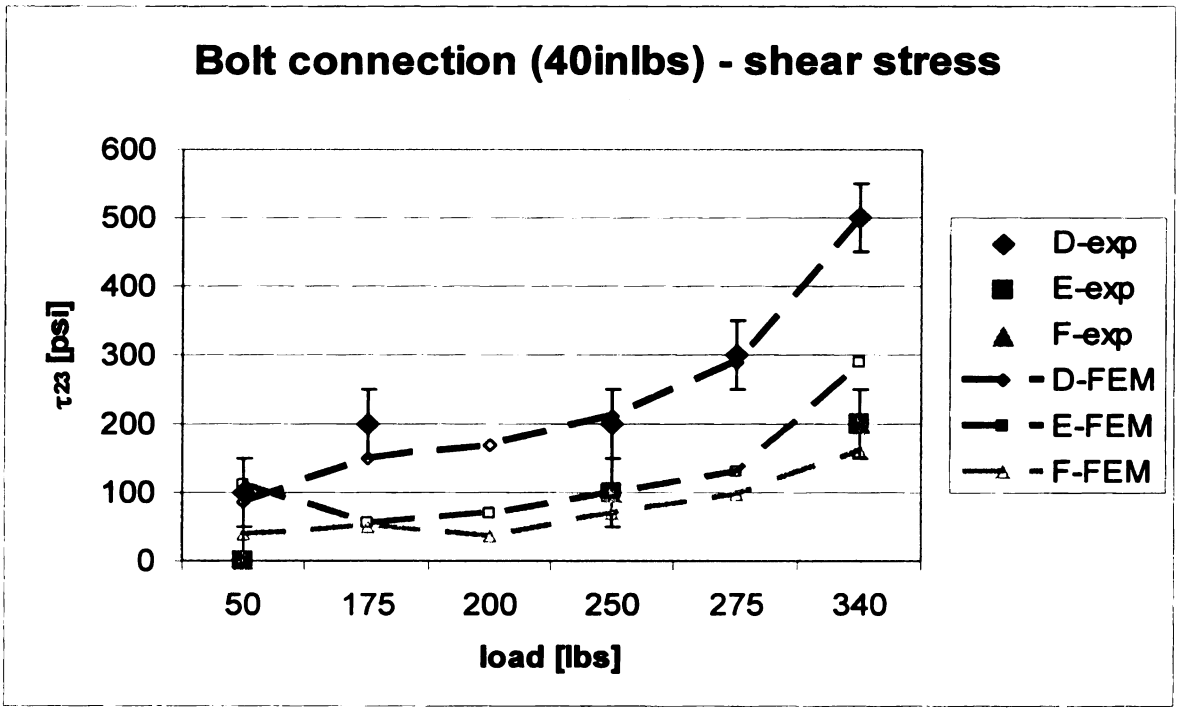

Figure 5.11 Shear stress in the bearing plane versus the load applied to the joint (bolt connected joint, 40 in-lbs torque).

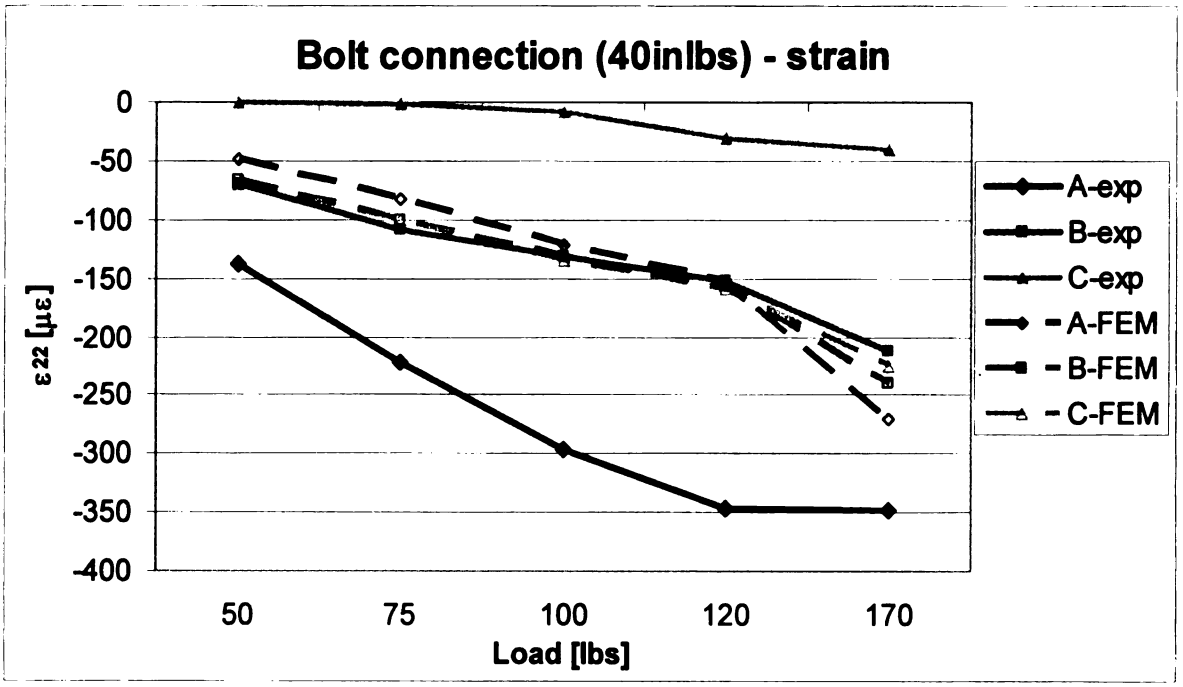

Figure 5.12 Normal strain in the bearing plane versus the load applied to the joint (bolt connected joint 40 in-lbs torque).

As can be seen from Figures 5.11 and 5.12, the same remarks as for 25 in-lbs torque can be made (see Figures 5.9 and 5.10), which leads to the conclusion that the numerical model provides consistent results.

Chapter 6

DISCUSSION OF RESULTS AND CONCLUSIONS

6.1. ALTERNATIVE JOINT DESIGNS FOR DECREASING THE MAXIMUM STRESS

To decrease the stresses in composite plate, two alternative designs were proposed and analyzed numerically. The first design includes a steel bushing around the hole in the plate. A section of the mesh of the plate can be seen in Figure 6.1.

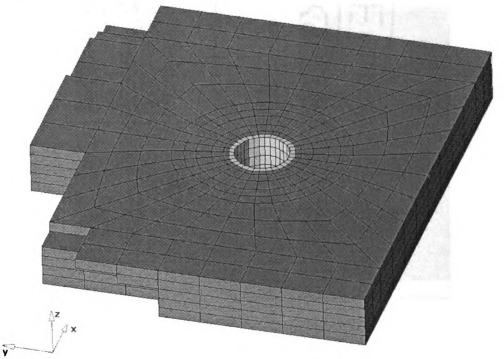

Figure 6.1. Typical mesh of the plate with a steel bushing around the hole (alternative design one).

The thickness of the bushing is 0.05 inches and the material has the following properties: E = 30 e6 psi and ν = 0.28. The role of the bushing is to take over the high stress concentration zone, since steel has a higher ultimate strength. Also, the steel bushing makes the plate stiffer in the longitudinal direction, and especially in the bearing zone.

The distribution of the shear stress in the bearing plane for this alternate design can be seen in Figure 6.2. This load case incorporates a 4 in-lbs torque on the bolt and 120 lbs loading of the joint.

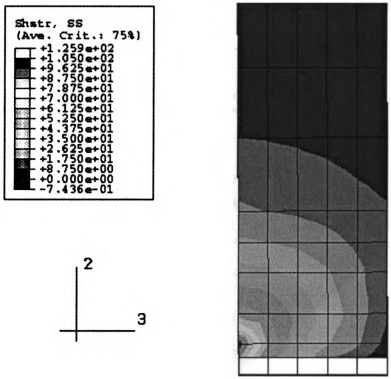

Figure 6.2 Distribution of shear stresses in the bearing plane of the modified resin plate for 4 in-lbs torque on the bolt and 120 lbs load on the joint (results are in psi).

As can be seen, a maximum stress of only 105 psi is developed inside the resin plate, while for a regular plate the stress is 230 psi. This design decreases the maximum stress in the bearing plane of the resin plate by 50 %. A comparison of the stresses and strains between the regular plate and the alternate designs can be seen in Figures 6.5 and 6.6.

The second model involves a 45 degrees chamfer of the edge of the hole. A portion of the mesh of this alternative design plate can be seen in Figure 6.3.

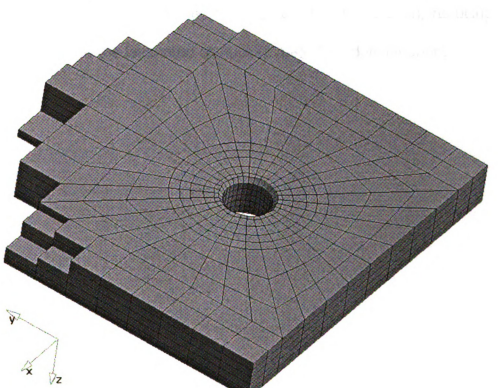

Figure 6.3. Typical mesh of the plate with a trim of the edge of the hole (alternative design two).

In the bearing plane, the maximum stress concentration is in the corner where the resin plate meets the aluminum plate and the bolt (see Figures 5.1 and 5.5). By chamfering that corner, which in fact trims the hole's edge, that stress can be distributed over a wider area. This will cause a reduction in the highest stress.

The results for this second design can be seen in Figure 6.4. Although the value of the maximum stress has not been lowered, its position has changed. Now, the maximum stress is in the middle of the bearing section, reducing the risk of cracking or, in the laminated composite materials, delamination.

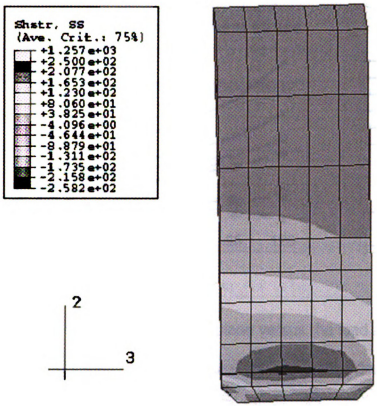

Figure 6.4 Distribution of shear stresses in the bearing plane of the modified resin plate for 4 in-lbs torque on the bolt and 120 lbs load on the joint (results are in psi).

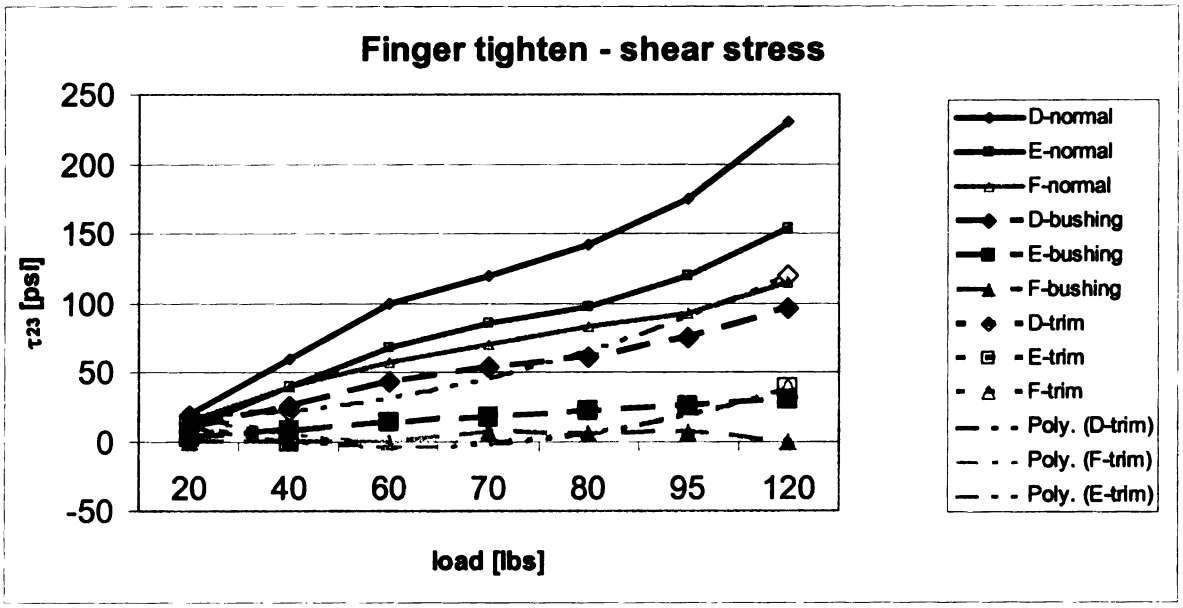

Figure 6.5. Shear stress in the bearing plane versus the load applied to the joint (finger tightened joint) for original and alternative designs.

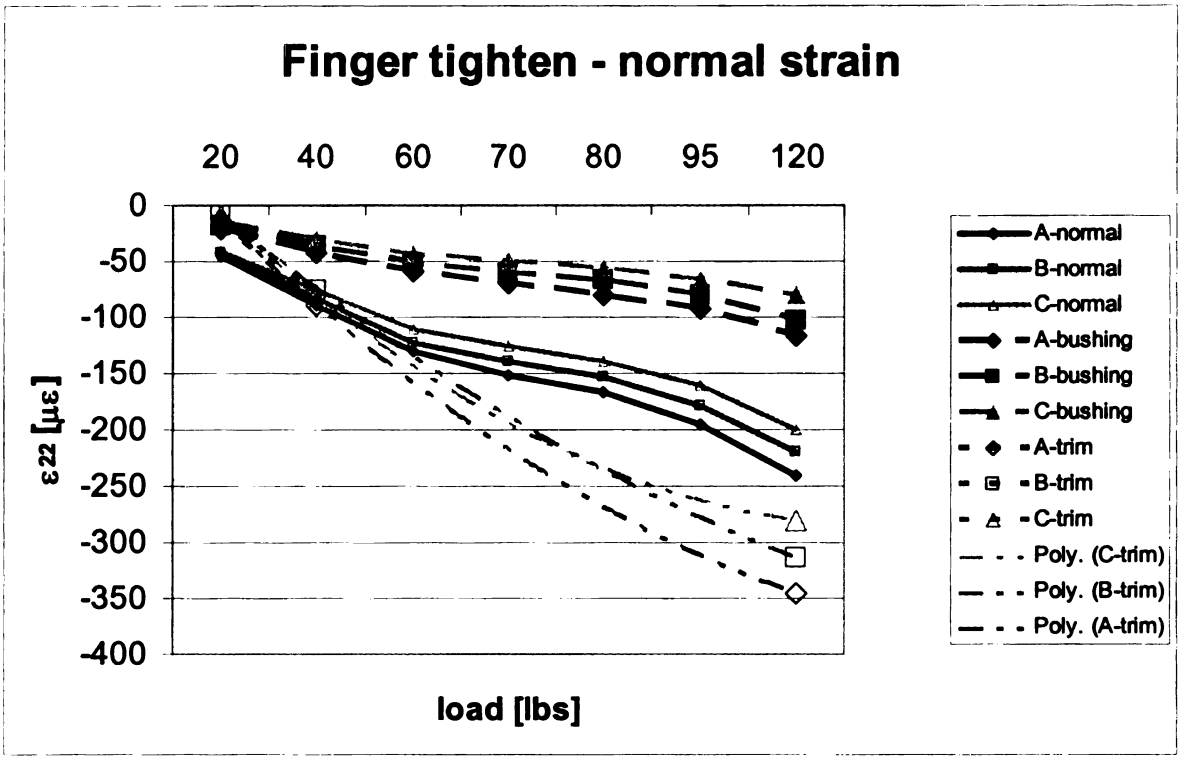

Figure 6.6. Normal strain in the bearing plane versus the load applied to the joint (finger tightened joint) for original and alternative designs.

6.2. SOURCES OF ERRORS

6.2.1. Strain gage errors

Errors in the strain gage measurements might be the induced by the mounting of the third strain gage. An air bubble was caught between the layers of the embedded polariscope, air bubble that can affect the strain measured. Figure 6.7 shows the air bubble.

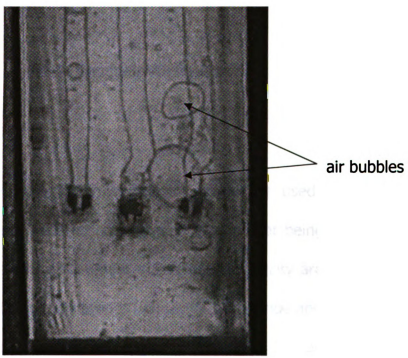

Figure 6.7. Bubbles inside the plate, next to the strain gage.

Another source of errors is the delamination of the investigated slice of material from the plate towards the end of the experimental measurements. This can lead to false measurements from the strain gages.

Also temperature can be a factor of errors, since the gages were temperature compensated only for the circuit. They were not setup to compensate the difference in the temperature of the resin plate, since the compensation gage was not embedded like the active ones.

6.2.2. Photoelasticity errors

As previously mentioned, the embedded polariscope used for measuring stresses inside the resin plate has the disadvantage of not being able to apply compensation. That is why all the results from photoelasticity are reported with ±50 psi error bars. Since the difference between a dark fringe and a white fringe gives a stress spread of 100 psi, and since shades of gray cannot be differentiated, the results have a potential error of 50 psi. The photoelasticity results have been reported only in the points of fringe change and a trendline added to the graph to get an approximate value in any point. It has to be mentioned that a trendline will not always provide the exact result, since the

variation of stresses with load is not linear nor does it follow any other mathematical function. Jumps in the values of stress can occur due to slippage between the plates.

6.2.3. Modeling errors

One problem in the FEA model is the force applied on the bolt head and nut, the force that simulates the clamping force. The force is applied on the z-axis (or 3-direction). But, in reality, as loading is applied on the joint and the two plates move with respect to each other, the bolt tilts, causing the loading to be at a certain angle to the 2-direction. As suggested in Figure 6.8 and 6.9, all the clamping force at the end of the loading case is applied on the 2-direction instead of being divided between 2- and 3-directions.

Also sensitivity to friction coefficient and material properties have to be taken into consideration when talking about errors. In the actual design, due to the step loading of the joint, slippage can occur instead of continuous motion between plates.

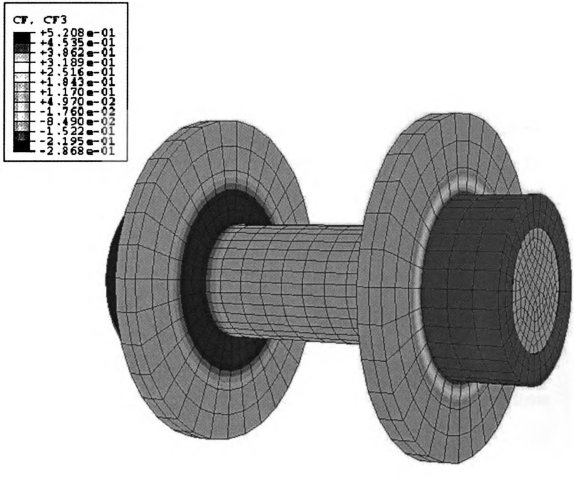

Figure 6.8. Nodal force applied on the 3-direction at the end of the load case.

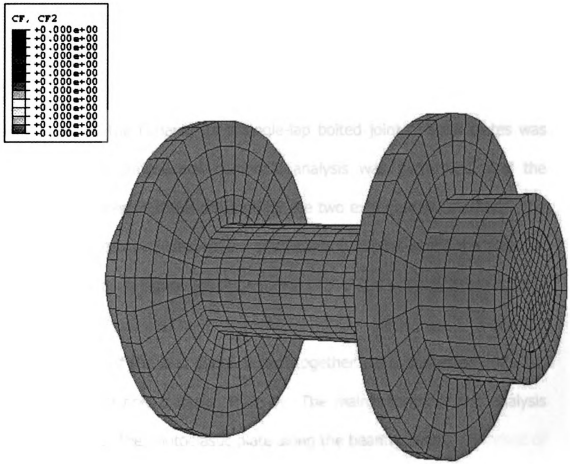

Figure 6.9. Nodal force applied on the 2-direction at the end of the load case.

6.3. CONCLUSIONS

In this study, the behavior of a single-lap bolted joint of thick plates was evaluated. A three dimensional numerical analysis was performed, and the results were compared to those obtained by the two experimental methods. The experimental methods provided values of stress and strains inside the plate on the bearing plane, as in Figure 3.2.

The materials of the two plates bolted together were aluminum 2024-T4, and photoelastic isotropic material, PSM -9. The main interest of this analysis was the stress inside the photoelastic plate along the bearing plane.

Experimental analysis was conducted via photoelastic investigations, by creating an embedded polariscope in the bearing plane of the plate. Additionally, resistance strain gages were mounted inside the plate along the same plane. The numerical modeling was performed with the Abaqus commercial code using material properties and other data obtained experimentally as input. The results were able to capture the behavior of the joint when loaded.

The maximum shear stress in the bearing plane of the photoelastic plate caused by the loading of the joint was created by tilting the bolt. It has been

proven that the higher the torque applied on the bolt, the lower the maximum stress in the plate. Yet, if a certain value of this torque is exceeded, failure of the joint will occur. The results can be seen in chapter 5, but some of them are summarized below.

For the pin connection the maximum shear stress given by FEA was 750 psi for 50 lbs load on the joint, while the photoelasticity result was 700 psi. That is an error of 7.14 %; taking into consideration that the photoelasticity results have 50 psi error margin, the difference between the numerical and experimental result vary from 0 to 7.14%.

The bolt joint, with a 4 in-lbs torque applied on the bolt, the equivalent of finger tightening, provided the following results. For 50 lbs load on the joint, the maximum stress was 80 psi, which is almost 9 times smaller than for the pin joint. The maximum stress for this clamping force, obtained experimentally, at a load of 95 lbs on the joint, was 200 psi, while the numerical value was of 175 psi. The difference is 12.6%.

For the 25 in-lbs torque applied to the bolt, which is the equivalent of 190 lbs distributed load in the FEA model, the following results were obtained. Maximum shear stress obtained experimentally was at 225 lbs and its value is

300 psi. The numerical result for the same loading conditions was 350 psi. The discrepancies range from 5% to 16.6%.

For 40 in-lbs torque, equivalent to 300 lbs in the numerical model, the maximum load was 340 lbs. Both the numerical and experimental results were 500 psi. The error varies from 0% to 13%.

Two other plates were designed in order to decrease the value of the maximum stress. The first plate presented a steel bushing around the hole, and the value of the stress in the epoxy plate was diminished by 50%. The second design presented had the edges of the hole chamfered at a 45 degree angle. This design didn't show a decrease in the maximum stress, but it showed a change in the position of the maximum stress, to a location less susceptible to cracking or delamination (in the case of laminated composite materials). Taking into consideration that the second design is just a little or no more costly than the original design, it is a good alternative for improving the bolt joining of the composite plates.

For the finger tightened bolt joint, at 120 lbs load on the joint, the original design displayed a stress of 230 psi in the corner of the slice (see Figure 5.5). The second design, with the steel bushing had a maximum calculated stress of 96 psi in the same loading conditions and the third one, with the chamfered

edges only 120 psi. Given the same loading conditions, the strains calculated in the position of the middle strain gage, were the following. For the original design 212 $\mu\varepsilon$, the second design 103 $\mu\varepsilon$, and the third one 313 $\mu\varepsilon$. This result proves that both the alternative designs need to be further investigated for a better understanding of their behavior, since they are both candidates to replace the original design.

The application of the force on the bolt has to be very closely regarded in the future, and a new method has to be found. If the force is applied to the bolt, then this force has to change its orientation together with the orientation of the bolt. Regarding the experiment, an important condition has to be fulfilled: the surfaces of the specimen have to be very smooth, since even the smallest irregularity will create a stress concentration recorded by photoelasticity method.

Future research will be concentrated on applying the same numerical model to laminated composite materials. The results will be verified with the experimental ones, since the development of a birefringent composite material is nearly completed.

REFERENCES

Altair Computing, Inc. (2001). HyperMesh user manual ver. 5.0, Altair Computing, Inc.

Barbero, E. J., Luciano, R. and Sacco, E. (1995). "Three-dimensional plate and contact/friction elements for laminated composite joints." Computer and Structures **54**(4): 689-703.

Camanho, P. P. and Matthews, F. L. (1996). "Stress analysis and strength prediction of mechanically fastened joints in FRP: a review." Composites Part A: 529-547.

Chen, W.-H., Lee, S.-S. and Yeh, J.-T. (1995). "Three-dimensional contact stress analysis of a composite laminate with bolted joint." Composite Structures **30**: 287-297.

Cloud, G. L. (1995). Optical methods of engineering analysis. New York, NY, Cambridge University Press.

Dano, M.-L., Gendron, G. and Picard, A. (2000). "Stress and failure analysis of mechanically fastened joints in composite laminates." Composite Structures **50**: 287-296.

Hibbitt Karlsson & Sorensen, Inc. (1998). ABAQUS/Standard user manual ver. 6.2. Pawtucket, RI, Hibbitt, Karlsson & Sorensen, Inc.

Huebner, K. H., Dewhirst, D. L., Smith, D. E. and Byrom, T. G. (2001). The finite element method for engineers. New York, NY, Wiley - Interscience.

Ireman, T. (1998). "Three-dimensional stress analysis of bolted single-lap composite joints." Composite Structures **43**: 195-216.

Ireman, T., Ranvik, T. and Eriksson, I. (2000). "On damage development in mechanically fastened composite laminates." Composite Structures **49**: 151-171.

Lin, H. J. and Tsai, C. C. (1995). "Failure analysis of bolted connections of composites with drilled and moulded-in hole." Composite Structures **30**: 159-168.

Lincoln, B., Gomes, K. J. and Braden, J. F. (1984). Mechanical fastening of plastics. An engineering handbook, Marcel Dekker, Inc./New York - Basel.

Matthews, F. L. (1983). "Design of bolted joints in GRP." Fibre-resin composite - new applications and development: 18-24.

Matthews, F. L., Davies, G. A. O., Hitchings, D. and Soutis, C. (2000). Finite element modelling of composite materials and structures, Woodhead Publishing Limited.

McCarthy, M. A., Lawlor, V. P., Stanley, W. F. and McCarthy, C. T. (2002). "Bolt-hole clearance effects and strength criteria in single-bolt, single-lap, composite joints." Composite Science and Technology **62**: 1415-1431.

Measurements Group, Inc. (1992). Student manual for strain gage technology.

National Instruments, Inc. (2000). LabView user manual 5.1, National Instruments.

Oh, J. H., Kim, Y. G. and Lee, D. G. (1997). "Optimum bolted joints for hybrid composite materials." Composite Structures **38**: 329-341.

Park, H.-J. (2001). "Effects of stacking sequence and clamping force on the bearing strengths of mechanically fastened joints in composite laminates." Composite Structures **53**: 213-221.

Parmley, R. O. (1977). Standard handbook of fastening and joining, McGraw-Hill.

Ramakrishna, S., Hamada, H. and Nishiwaki, M. (1995). "Bolted joints of pultruded sandwich composite laminates." Composite Structures **32**: 227-235.

Savicki, A. J. and Minguet, P. J. (1997). Failure mechanisms in compression-loaded composite laminates containing open and filled holes. Philadelphia, The Boeing Company.

Speck, J. A. (1997). Mechanical fastening, joining and assembly, Marcel Dekker, Inc.

Starikov, R. and Schon, J. (2001). "Quasi-static behaviour of composite joints with protruding-head bolts." Composite Structures **51**: 411-425.

Starikov, R. and Schon, J. (2002). "Experimental study on fatigue resistance of composite joints with protruding-head bolts." Composite Structures **55**: 1-11.

Starikov, R. and Schon, J. (2002). "Local fatigue behaviour of CFRP bolted joints." composite Science and Technology **62**: 243-253.

Tong, L. (2000). "Bearing failure of composite bolted joints with non-uniform bolt-to-washer clearance." Composites: Part A **31**: 609-615.

Ugural, A. C. and Fenster, S. K. (1995). Advanced strength and applied elasticity. New Jersey, Prentice Hall.

Wang, W.-C. and Sheu, Y.-M. (1996). "Stress analysis of bolted joints in CFRP laminates by half-fringe birefringent-coating technique." Composite Structures **34**: 91-100.

Zetterberg, T., Astrom, B. T., Backlund, J. and Burman, M. (2001). "On design of joints between composite profiles for bridge deck applications." Composite Structures **51**: 83-91.